Developing a Three Stream, Mixed Flow Variable Cycle Engine in NPSS

Vincent Larsson

DEPARTMENT OF MECHANICS AND MARITIME SCIENCES
Chalmers University of Technology
Gothenburg, Sweden 2023
www.chalmers.se

Acknowledgements

I would like to express my sincerest gratitude to the people at GKN Aerospace in Trollhättan who granted me the opportunity to work on this thesis. In particular I'd like to thank my two supervisors Patrick Nilsson and Anna Nyhlén; thank you for your patience with the project and for providing the invaluable guidance and expertise that enabled me to push this thesis past the finish line. Working under your supervision has been a great and rewarding experience. I also want to sincerely thank my examiner Tomas Grönstedt for his help and commitment along the way, without which my work may well have yet to be completed.

Tack Stina, för hur du har stöttat mig.

Abstract

One of the more important areas of improvement in aircraft engines is fuel efficiency for economic as well as environmental reasons. While modern civil turbofan engines are primarily designed with fuel efficiency in mind, thus having very high bypass ratios, military engines need to uphold high specific thrust requirements in order to reach supersonic speeds as well as perform the manoeuvres sometimes necessary in a combat scenario. Modern military aircraft engines are therefore designed as low-bypass turbofans capable of producing significant specific thrust, but at the cost of having a high specific fuel consumption even at lower speeds in comparison to their civil counterparts.

The variable cycle engine, or adaptive cycle engine, is an engine concept for which the engine cycle can be modified in-flight to better fulfil different mission requirements. The type of variable cycle engine of interest for this thesis is a so called three stream, double bypass, mixed-flow variable cycle engine, in which a low-bypass turbofan engine has had an additional outer bypass duct added to it. This third stream can be independently modulated to vary the bypass ratio of the engine during flight, increasing the airflow through the bypass duct during subsonic flight for better fuel efficiency and increasing the flow through the engine core during supersonic flight for higher thrust.

For the thesis, the Numerical Propulsion System Simulation software (NPSS) was used to both model and simulate two variable cycle engines with differing design bypass ratios. In order to evaluate the models, a baseline model representing a generic, standard low-bypass turbofan engine was also modelled for comparison. The primary area of study for the models was the effect of increased bypass ratio on thrust specific fuel consumption at different altitudes and speeds, as well as the total fuel savings during a simulated mission. The results showed that overall, the variable cycle engines had an advantage over the standard engine with regard to fuel consumption during dry-thrust. The mission analysis performed showed possible fuel savings of ca. 11 and 14 % compared to the base model for the two VCE designs respectively. This came however at the expense of a lower maximum net thrust when operating at wet-thrust settings.

Contents

Nomenclature

$\dot{m}$	Mass Flow Rate
$\dot{m}_a$	Mass Flow Rate of Air
$\dot{m}_f$	Mass Flow Rate of Fuel
$\dot{Q}_{in}$	Thermal Energy Release Rate
$\dot{W}_{out}$	Net Power Output
η_{is}	Isentropic Efficiency
η_O	Overall Efficiency
η_{pol}	Polytropic Efficiency
η_P	Propulsion Efficiency
η_T	Thermal Efficiency
γ	Heat Capacity Ratio of Air
γ_{comb}	Heat Capacity Ratio of Combustion Gases
π_c	Compressor Pressure Ratio
π_t	Turbine Pressure Ratio
ACE	Adaptive Cycle Engine
BPD	Bypass Duct
BPR	Bypass Ratio
$BPRdes$	Design Bypass Ratio
EPR	Engine Pressure Ratio
F_g	Gross Thrust
F_n	Net Thrust
FAR	Fuel Air Ratio
$FDCS$	Fan Driven Core Stage
FPR	Fan Pressure Ratio
HPC	High Pressure Compressor
HPT	High Pressure Turbine
$IBPR$	Inner Bypass Ratio
LPC	Low Pressure Compressor
LPT	Low Pressure Turbine
$NPSS$	Numerical Propulsion System Simulation
$OBPR$	Outer Bypass Ratio
OPR	Overall Pressure Ratio
PLA	Power Lever Angle

PR	Pressure Ratio
rpm	rounds per minute
SFC	Specific Fuel Consumption
SLS	Sea Level Static
$TBPR$	Total Bypass Ratio
TL	Technology Level
V	Flight Velocity
V	Velocity
V_j	Jet Velocity
$VABI$	Variable Area Bypass Injector
VCE	Variable Cycle Engine

1 Introduction

1.1 Background

Modern military aircraft are required to fulfil a wide range of operational needs placed upon them during differing flight conditions, meaning that the engine will operate with greatly varying thrusts. The demands placed on maneuverability, acceleration and high maximum velocity for fighter aircraft mean that the engine must be capable of achieving a high specific thrust. In contrast to civil aircraft engines, fighter engines are for this reason designed as low bypass turbofans which produce a higher jet velocity in turn leading to a high thrust per unit mass flow of air [1]. A high specific thrust is however directly correlated to a high specific fuel consumption (SFC), that is, the amount of fuel consumed per unit of thrust produced [2]. Due to its engine architecture, the specific thrust and SFC remain high for a low-bypass turbofan even at lower thrusts.

In an effort to improve the fuel economy while preserving the capability for high specific thrust, research into the concept known as a variable cycle engine (VCE), or adaptive cycle engine (ACE), has been conducted ever since the 1950s [3]. While different concepts for VCEs exist, the type of VCE in question for this thesis would accomplish these otherwise conflicting requirements by varying the bypass ratio (BPR) in flight, passing more or less air past the engine core depending on the thrust required. For this thesis, the potential benefits of adding a second bypass stream to a low bypass turbofan engine will be investigated. This will be accomplished by using the NPSS software to model a baseline, low bypass turbofan engine with an afterburner which represents a standard military engine in use today. With the base model as a starting point, a VCE will then be modelled by modifying the engine architecture of the base model to include, among other things, a second bypass stream. The capabilities of the models in terms of fuel consumption and thrust output will then be compared through a series of simulation sweeps and a mission analysis.

1.2 Purpose and Aim

The aim of the thesis is to use NPSS to develop a model representing a three stream, variable bypass VCE. The model is then to be evaluated to assess the benefits of the added third stream in terms of performance. The following objectives should ideally be accomplished:

- Conducting a literature study in order to identify similar work and to gain a general understanding of the subject matter, including but not limited to how methods may be implemented.
- Development and simulation of a three-stream, variable bypass VCE in NPSS.
- Simulation of the VCE within an operating envelope and a predefined mission to evaluate performance.
- Comparison to conventional engine architecture and assessment of the variable bypass performance benefits.
- Development and optimisation of a control schedule to modulate the variable bypass third stream of the VCE.
- Comparison between different component design input data (efficiencies etc.) based on technology level and assessing their impact on performance.

1.3 Limitations

The scope of the thesis will be limited to only conducting simulations and analysis on steady state performance. Moreover, this thesis will only cover the uninstalled performances of the models without parameters such as engine weight and size, ram pressure recovery, spillage drag, etc. being considered. Lastly, the engines will only be modelled to the extent that the most basic components are included, without going into the finer details of how the real engines would be designed and constructed.

1.4 Theoretical Framework

In the sections following below, some basic types of jet engines will be described briefly along with some important equations and concepts necessary to understand the motivation behind VCEs.

1.4.1 Turbojet Engines

The turbojet is the oldest of the existing jet engine types, with its first development dating as far back as the late 1930s. The turbojet has the overall best performance for supersonic flight, though aircraft designers have increasingly opted for using turbofans instead of turbojet engines in civil as well as military aircraft due to the fuel economy gains at subsonic speeds [3]. In Figure 1 below, the basic engine architecture can be seen.

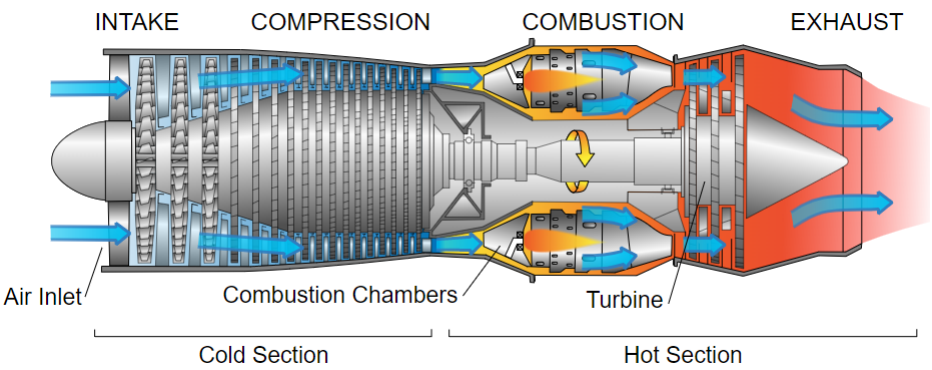

Figure 1: Schematic of a basic turbojet engine [4] .

The thrust of a turbojet is created via combustion of compressed air mixed with fuel in the combustion chamber, thereafter expanding it through the turbine and the nozzle. Having no bypass duct, all the airflow in the turbojet passes through the core of the engine. This gives it a high specific thrust which, assuming perfect expansion in the nozzle, is defined as

$$\frac{F_n}{\dot{m}_a} = (1 + FAR) * V_j - V \ (m/s) \tag{1}$$

where F_n is the net thrust, $\dot{m}_a$ is the mass flow rate of air, FAR is the fuel/air ratio, V_j is the jet velocity and V is the flight velocity. High specific thrust corresponds to high SFC, which is given by

$$SFC = \frac{\dot{m}_f}{F_n} \ (kg/(kN * s)) \tag{2}$$

where $\dot{m}_f$ is the fuel mass flow. To understand why this is the case, the measurements of efficiency for an aircraft engine will be introduced as well. First is the engine cycle efficiency, or overall efficiency, (η_O), which is the thermal efficiency (η_T) multiplied by the propulsive efficiency (η_P)

$$\eta_O = \eta_T * \eta_P \tag{3}$$

The thermal efficiency is defined as the net rate of shaft power, or kinetic energy, produced by the engine divided by the thermal energy of the fuel [5]. In equation form, it is written as

$$\eta_t = \frac{\dot{W}_{out}}{\dot{Q}_{in}} \tag{4}$$

where $\dot{W}_{out}$ is the net power output and $\dot{Q}_{in}$ is the rate of thermal energy released. The second type of efficiency is the propulsive efficiency, which is defined as

$$\eta_P = \frac{F_n * V}{\dot{W}_{out}} \tag{5}$$

For a case in which a much smaller $\dot{m}_f$ than $\dot{m}_a$, perfect expansion, and very small installation losses are assumed, the equation for propulsive efficiency simplifies to

$$\eta_P = \frac{2}{\frac{V_j}{V} + 1} \tag{6}$$

It can now be readily seen that the propulsive efficiency is maximized when the V_j is minimized, which is why a high bypass turbofan engine which accelerates large amounts of air at a comparatively low velocity is more efficient than a turbojet or low bypass turbofan accelerating air at high velocity.

1.4.2 Turbofan Engines

The turbofan engine is an engine working on the same basic principle as the turbojet, with compressed air being combusted and expanded to generate thrust. The key difference between them however, is that while the turbojet would use all (minus what is required to power the compressor) of the available energy to accelerate the jet stream, the turbofan uses a significant amount of that same energy to provide additional shaft power to the large fan in the front. Usually, the compressor and fan are situated on different shafts, being connected to the high and and low pressure turbines via their respective shafts. The fan propels air at relatively low velocity, with the flow being split between the core stream and the bypass stream, producing thrust at a high propulsive efficiency.

Below in Figure 2 is shown a simple schematic of a basic turbofan engine.

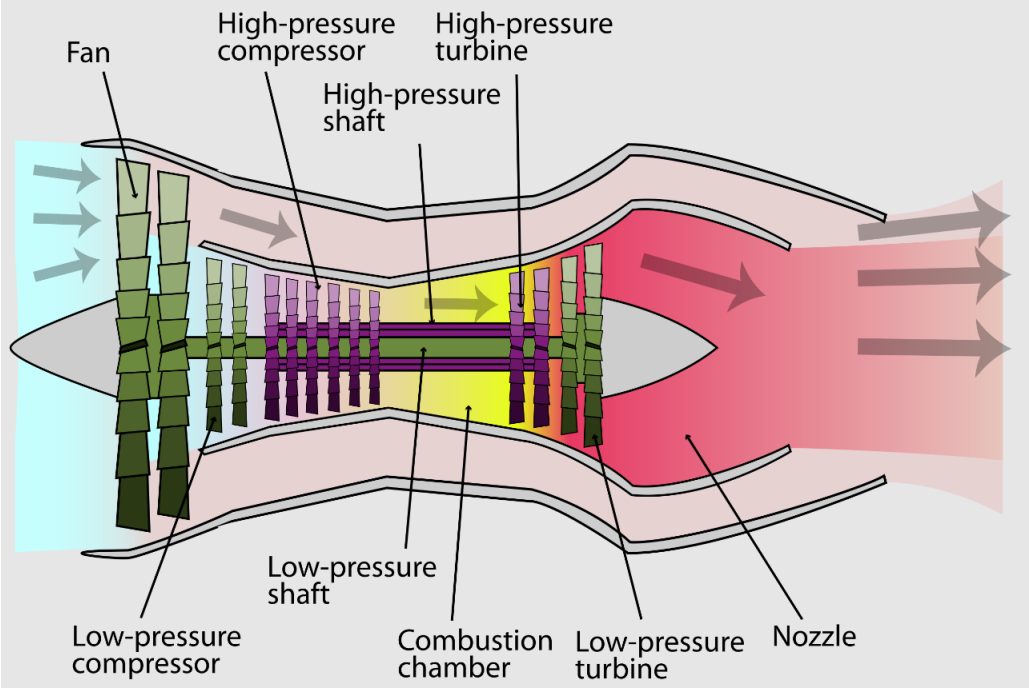

Figure 2: Schematic of a basic turbofan engine [6].

Most fighter engines have since the 1960s been so called low bypass turbofans with a single bypass duct and a BPR between 0.3 and 1.0 [3]. For civil aircraft, turbofan engines are usually designed for a BPR of 10 or more, which contrasts starkly with the aforementioned BPR of fighter aircraft. The bypass ratio is defined as the mass flow of air going through the bypass duct divided by the mass flow of air going through the engine core. Here it is shown in equation form:

$$BPR = \frac{\dot{m}_{a,bypass}}{\dot{m}_{a,core}} \tag{7}$$

With the maximum thrust that may be required during a mission being more than ten times higher than the minimum thrust when loitering, the fighter aircraft engine has a lot of variability to handle [1]. Whether the engine being of the turbofan or turbojet type, a solution to this variability is to include an afterburner in the design. The afterburner is an additional combustor placed between the last turbine and the nozzle, combusting extra injected fuel to further heighten the temperature and therefore velocity of the combustion gases. When engaged, this dramatically increases thrust at the expense of SFC. When the engine is operating with the afterburner turned on, it is called wet thrust as opposed to dry thrust where the engine operates without the afterburner. For fighter aircraft, operating at wet thrust would only be taking place at certain points in the operational envelope, such as at takeoff and at speeds in the high supersonic range [7].

1.4.3 Spillage Drag

Finally, before moving on to describing VCEs, spillage drag will be introduced briefly since this is an important motivation behind the development of VCEs.

Spillage drag is what results from air which does not enter the engine, but is accelerated by the engine nacelle's surrounding static pressure field [7]. The air is "spilled" around the outside instead of travelling to the compressor face, thus creating a drag force [2]. An engine inlet is usually sized to

accommodate the maximum airflow that the engine could possibly demand, and the phenomenon of spillage drag thus occurs when operating the engine below this maximum airflow; the power setting of the engine and incoming airflow are reduced, but the inlet capture area is unchanged.

For civil aircraft, this is less of a problem since they typically operate at constant settings close to the design conditions. For military aircraft however, this naturally becomes a problem since the inlet is designed for the maximum airflow required at high thrust settings. The aircraft will then spend much of its time cruising at part power settings with a considerably lower airflow as a result.

1.4.4 Variable Cycle Engines

The VCE concept has since its inception more or less been an attempt to incorporate desirable elements from the turbojet and turbofan into one, i.e. an engine capable of producing high specific thrust when required but with the ability to increase its propulsive efficiency at lower speeds. To produce higher specific thrust, a larger share of the airflow would be directed through the core of the engine to maximise the velocity out of the nozzle, making the engine function more akin to a turbojet. At part power setting however, it does the opposite and redirects larger proportions of the air to bypass the core entirely, operating more similarly to a high bypass turbofan. Furthermore, the VCE could also pose a partial solution to the problem with spillage drag described previously. Should the VCE be able to operate at reduced power/thrust and maintain a high airflow by directing it through the bypass ducts(s), then the effect of spillage drag will be lessened, in turn further reducing the SFC at lower thrust settings.

Work on developing a suitable VCE has been going on at General Electric ever since 1960, and several differing concepts have since been investigated [3]. For the sake of not bloating the report, this section will be limited to describing the ones most relevant to this thesis, i.e. the ones stemming from the modulating bypass (MOBY) concept.

The first of these VCEs was the three spool modulating bypass ratio VCE-MOBY developed in 1973 to address the problem of inlet and afterbody drag at reduced thrust [8]. The engine had three spools, variable area turbines and variable area nozzle throats as well as two variable area stator fans and bypass ducts [8]. In a regular mixed flow turbofan engine, the total pressures at the core and bypass stream mixing plane must be kept in balance as to avoid losses in the engine. To exemplify what would happen if there is too great an imbalance, imagine for instance an engine where the bypass stream has a lower pressure than the core stream at the mixing point. Part of the core flow would then begin to travel backwards toward the lower pressure, i.e. into the bypass duct, which is of course highly undesirable. With three nozzles, this engine design is a separate flow one which avoids the constraint of balancing the static pressures in the mixing planes of the core and bypass streams. This allows for more operational flexibility as opposed to a mixed flow turbofan - the trade-off being increased complexity. The engine runs practically as a standard two stream turbofan at max power, with the outermost bypass duct being almost closed to airflow. At part power settings, the operating mode of the front fan is set to match the inlet requirement of the engine while the second and third spool speeds are varied to reduce the thrust [3]. Front fan flow could thus be maintained at low thrust levels by simply gradually increasing the share of airflow diverted from the core stream to the bypass streams. This engine concept was successful in mitigating spillage drag and installation losses, thus achieving high performance - particularly at part power settings. Alas, the high complexity added by the additional nozzles, ducts and spools made its practicality questionable.

In 1976, a way to tackle the conflicting requirements of reducing the complexity of a three stream, double bypass VCE and maintaining the static pressure balances in the core and bypass stream mixing points was devised [3]. The concept in question is called a Variable Area Bypass Injector (VABI). A VABI adjusts the inlet areas of the core and bypass streams to their respective mixing planes, thereby adjusting the total pressure of each stream. In a double bypass VCE, installing VABIs at the mixing planes of the streams would allow for a VCE with mixed flow and a single

nozzle, resulting in a much simplified engine architecture while maintaining most of the cycle advantages of a fully separated flow VCE [3].

In his dissertation *Design and Control of a Variable Geometry Turbofan with an Independently Modulated Third Stream*, Simmons has used NPSS to model an engine concept somewhere in between the two described VCEs - a three stream, double bypass VCE with two variable nozzles and a VABI [9]. The VABI is located at the mixing plane of the inner bypass stream and the core stream while the outer bypass stream exits the engine through a separate nozzle. The motivation for this sort of hybrid engine architecture is that while the VABI reduces the complexity of the engine, the second nozzle allows the engine to operate at even lower power settings [9]. Using mission analyses to evaluate the engine, the results obtained were very promising with fuel savings being estimated at over 30 % compared to a reference turbofan engine [9].

The engine modelled in this thesis is a three stream, double bypass mixed flow configuration, the details of which will be discussed more closely in the next chapter.

1.4.5 NPSS - General and Model Configuration

Numerical Propulsion System Simulation (NPSS) is

> " an object-oriented, multiphysics, engineering design and simulation environment that enables development, collaboration and seamless integration of system models [9, p. 5]."

The software is developed by the National Aeronautics and Space administration (NASA) and is intended for cycle design and analysis of gas turbine engines - steady state and/or transient. For this thesis, the modelling and analyses conducted will be of the steady state kind.

A model in NPSS consists of different interconnected elements and subelements - objects representing engine components - with each element containing its own variables, functions and eventual subelements [10]. NPSS comes with a selection of premade elements and subelements which cover the most important functions found in a gas turbine engine, but the user also has the option to either modify these existing elements and subelements or make their own from scratch. One or more solver objects drive the model to a converged state, i.e, calculates a solution for all the elements. Should one wish to do so, the entire model could be configured in a single file. It is however more convenient to separate the model into several input files, e.g. a file for the model elements, a file for model execution and, a file for solver settings and so on, which in the end are all called upon in an executive file.

The first thing to be done before configuring the model, is to specify the thermodynamic package to be used [11]. This determines the fluid properties such as enthalpy, thermal conductivity etc., from known conditions of the fluid state, e.g. pressure and temperature [12]. The model is thereafter configured by instantiating all the objects (elements) that represent the engine components, such as compressors and turbines. The elements are preferably instantiated the order through which the fluid flows through the engine, since the the solver by default calculates the solutions for the elements in the the same order that they appear in the code. The elements are then finally linked together by specifying the inlet and outlet ports (fluid and shaft). For example, the burner outlet is linked to the turbine inlet, which in turn has a fluid connection to an element downstream as well as a shaft connection to the compressor upstream.

1.4.6 NPSS - Design and Off-Design Mode

Running the model is done in either design mode or off-design mode. A design mode run must always precede any off-design one, since this is where the engine geometry, i.e. the size of the components, is determined. Every off-design run does not however need to be preceded by a unique design run; each design run can rather be used as the base for an indeterminate number of off-design runs. When modelling an engine, the user must thus provide some design conditions for the elements instantiated. These conditions are reference conditions which may include altitude, flow Mach numbers, pressure ratios, efficiencies etc.

In off-design mode, the model is run at different conditions than the ones set in design mode. This could for example entail a difference in altitude and/or flight Mach number. The NPSS solver thus uses the geometry established in design mode to calculate the resulting component performances for the off-design conditions.

1.4.7 NPSS - Solver

The solver is an object in NPSS that is used to drive the the model to a converged state, attaining a physically valid solution [12]. Solver objects can be divided into three main types - independents, dependents and constraints. In some elements, these may already be present while others may be user instantiated. Independents are parameters that are varied in order to drive the model to convergence while dependents are conditions - equality statements - that determine the convergence [13]. The number of independents and dependents in the model must be equal. Constraints are a specific case of dependents that limit specified variables to a minimum or maximum value [13]. To show more what dependents and independents may look like in NPSS, see the following below:

- Independent instantiation:
  ```
  Independent independentName; {
  varName = "name of variable";
  }
  ```
- Dependent instantiation:
  ```
  Dependent dependentName; {
  eq_rhs = "variable parameter 1";
  eq_lhs = "variable parameter 2";
  }
  ```

The independents and dependents are not automatically added to the solver when instantiated; this must be done by the user with the appropriate commands. When the simulation is run, the NPSS solver will evaluate all calculations to be performed in the model according to the solver sequence. If the user wishes for the solver to to be another than the default one, this may be specified with a separate command. The NPSS solver follows an iterative procedure where after the calculations, the solver checks the convergence criteria (dependent variable conditions) where after it adjusts the independent variables. The solver repeats this cycle until all the convergence criteria are met.

2 Methodology

2.1 Overall Approach to Design and Modelling

The modelling process in NPSS and the parts that make up a model will first be explained in this section, in order for the reader to better be able to understand the designs.

2.2 Model Elements

Below follows Table 1 with all elements used in the NPSS models for this thesis listed. Note that the elements only included in the base model are bold faced, while the elements only appearing in the VCE model are in italic. Any element that is neither boldfaced nor italicized is present in both the base model and VCE model.

Table 1: The different elements included in the models. Elements only included in base model are bold faced while elements included only in the VCE models are in italic.

Element Name(s)	Element Type	Short Description
Amb	Ambient	Defines/calculates flight condition properties. No output port exists, requiring element InletStart to start the flow.
InletStart	InletStart	Sets inlet start conditions for flow to a downstream inlet based on variable parameters provided by Ambient element.
InEng	Inlet	Calculates performance of standard inlet after ram recovery.
SpltFan, ***SpltCmpH***	Splitter	Splits the entering stream into two outlet streams.
CmpFPri, **CmpFSec**, ***CmpFan***, ***CmpL***, CmpH	Compressor	Compresses the flow. Used with a map subelement.
D025, D060, D130, ***D230***	Duct	Calculates a pressure drop.
B030, B041, B045, B050	Bleed	Extracts a bleed flow from the main stream or reintroduces the same to the main stream.
FusPri, FusAug	FuelStart	Starts a fuel flow. Required for defining burner fuel properties.
BrnPri, BrnAug	Burner	Performs burner performance calculations, working with an entrance fluid stream and a fuel stream.
TrbL, TrbH	Turbine	Extracts energy from incoming flow through expansion, powering a shaft element. Used with a map subelement.
ShL, ShH	Shaft	Provides mechanical connection between rotating elements, e.g. compressors and turbines.
MixExh, ***MixNoz***	Mixer	Mixes two inlet streams together into one outlet stream.
NozMix	Nozzle	Calculates performance for nozzles, either convergent or convergent-divergent with either fixed or variable areas.
FeMix	FlowEnd	Terminates the stream.
EngPerfMod	EngPerf	Calculates overall engine performance parameters, e.g. F_g F_n, SFC etc.
Cycle	Cycle	Calculates the engine cycle parameters EPR, OPR FPR and BPR.

2.2.1 Ambient

Based on input variables, the Ambient element calculates flight condition properties such as altitude, ambient pressure and temperature and similar [14]. Examples of input variables can be Mach number and altitude. The element contains atmospheric tables of temperatures and altitudes for different vapor pressures, relative humidity, day types etc [13]. The element has no outlet ports, requiring an InletStart element to be useful.

2.2.2 InletStart

This element defines the starting conditions for the downstream inlet element, depending on the existing Ambient element to do so [13]. The name of the Ambient element is a required input, but

another typical input is the design inlet flow.

2.2.3 Inlet

The Inlet element carries out performance calculations for a standard inlet, including pressure drop and drag calculations based on ram recovery and ram drag respectively [13]. The inlet has a single inlet and outlet port, and must be preceded upstream by an element that provides flow, e.g. InletStart [14].

2.2.4 Splitter

The element Splitter divides the incoming stream into two outlet streams, thus having one inlet port and two outlet ports. The division of the flow to the two outlets is determined by the BPR, which is an output in design mode (set equal to design BPR, BPRdes, put in by user). In off-design mode, the BPR is an input if the element's independent variable ind_BPR is inactive [13]. By default, the element's independent variable ind_BPR is active during off-design, meaning that the NPSS solver will vary BPR, making it an output [14].

2.2.5 Compressor

Powered by the shaft element, the Compressor element compresses the incoming airflow with its performance calculated in terms of efficiency and stagnation pressure ratio (overall pressure ratio) [14]. In design mode, the design pressure ratio PRdes is required as a user input [13]. It is customary to use a compressor map subelement with the Compressor element, as is also the case for the models in this thesis.

2.2.6 Duct

The Duct element simply performs an adiabatic pressure loss calculation - either through a pressure calculation socket, the S_dP socket, or via user input [14]. The element adds the pressure loss without affecting the stream's enthalpy, which is maintained at a constant level [14].

2.2.7 Bleed

The Bleed element has two functions. It either extracts a bleed flow from the main stream, or reintroduces an existing bleed flow back into the main stream [14]. This can for example be relevant to provide internal cooling to the engine.

2.2.8 FuelStart

The FuelStart element initiates a fuel stream to a Burner element and determines the fuel properties in said Burner, similarly to how the InletStart element initiates the inlet stream to the Inlet element [13]. The element has default values for different element (that is, carbon, hydrogen etc.) mass-fractions, lower heating values and storage pressures already in place but allows the user to manually specify these as well.

2.2.9 Burner

The Burner element conducts burner performance calculations working with an entrance fluid as well as a fuel stream from the FuelStart element [14]. It mixes the two inlet flows together and determines the increase in temperature as combustion takes place, as well as calculates the pressure loss going into the burner based on dPqP (NPSS pressure drop variable) input by the user.

2.2.10 Turbine

A Turbine element expands an incoming stream, providing power to a Shaft element. The element conducts performance calculations to determine performance efficiency and either stagnation pressure ratio or enthalpy change [13]. The performance is calculated with said efficiency and pressure ratio/enthalpy change either directly assigned by the user, or assigned via a turbine map subelement [14].

2.2.11 Shaft

The Shaft element connects rotating elements in the model, e.g. a turbine and a compressor. In design mode, the shafts' rpm value is set as a user input. This element maintains the power balance between any components connected to it, and is not limited to a single connection per shaft element [13]. It can on the contrary have as many input ports, connecting several elements via the same shaft, as the user would like.

2.2.12 Mixer

A Mixer element combines two incoming flows into one, preserving energy and momentum as it does so [14]. A design Mach number for the primary inlet must be provided by the user in design mode, which will determine the entrance area. The element will thereafter solve for the secondary inlet entrance area by varying its inlet Mach number until the difference between the static pressures in the two inlets is within an acceptable range.

2.2.13 Nozzle

The Nozzle element carries out performance calculations for two types of nozzles, convergent or convergent-divergent, with the type being specified by the user. In the case of this thesis that deals with engines capable of supersonic flight, a convergent-divergent nozzle is used. The calculations require a specified exhaust pressure [13]. The exit area of the nozzle can either be specified to be a fixed one or a variable one, with the latter of these two used for this thesis. The Nozzle element will thus perform an exit area calculation that provides perfect expansion of the incoming flow to the exhaust pressure specified [14].

2.2.14 FlowEnd

The FlowEnd element has a single input port and no output ports. Its sole purpose is to terminate the flow stream of the model.

2.2.15 EngPerf

The EngPerf element calculates the following engine performance parameters: total engine F_g and F_n (gross and net thrust), F_{nc} (corrected net thrust), F_{ram} (ram drag), F_d (installation drag), W_{fuel} (total fuel flow), SFC and pwrSD (delivered shaft power) [14]. This element should be put last or near the end of the solver sequence, and no linkage is required to any other model element.

2.2.16 Cycle

The Cycle element carries out calculations to determine engine cycle parameters [14]. For the models in this thesis, these include BPR, EPR, FPR, and OPR. As with the EngPerf element, no linkage to other model elements is required.

2.3 Design of Base Model

Below will follow a description of the base turbofan model to which the VCEs will be compared. A flowchart of the model layout with all the NPSS components listed in Table 1 is shown below in Figure 3. Note that that the compressor and turbine elements are named differently than what is referenced in the table, in order for the text to fit within the elements.

2.3.1 Model Configuration

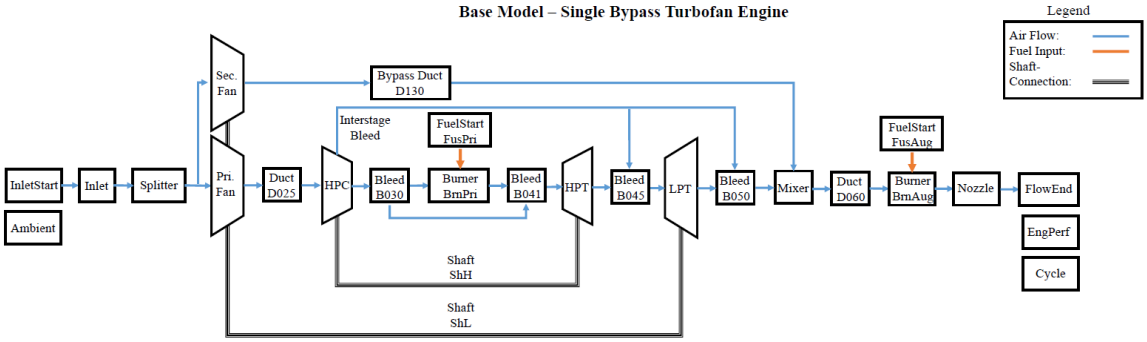

Figure 3: Flowchart of Base Model

The engine configuration is a two spool one, i.e. an engine with two shafts - one low pressure and one high pressure. The fan and low pressure turbine (LPT) are connected via the low pressure shaft while the compressor and high pressure turbine (HPT) are connected via the high pressure shaft. For this model, the fan section was divided into two components, CmpFPri and CmpFSec, with the latter having a somewhat higher design pressure ratio. This is to represent the slightly higher enthalpy increase taking place closer to the fan tip compared to the fan hub. The two fan components also divide the flow between the core and the bypass flow.

The stream starts to the far left at the element InletStart, which has data provided to it by the Ambient element. Next, the flow enters the Splitter element SpltFan which splits the incoming flow to the two fan segments, CmpFPri and CmpFSec. BPRdes is set at 0.5, meaning that one third of the flow goes through the secondary fan segment.

The flow out of CmpFSec goes to the bypass duct D130, which leads the airflow to the Mixer element near the end of the model. The flow out of CmpFPri leads to the high pressure compressor, CmpH. Two bleed streams are taken from the compressor - one interstage bleed and one bleed, B030, at the outlet. These streams provide internal cooling for the engine, with the interstage-bleed stream reentering the main stream via the Bleed elements B045 and B050, at the outlets of the HPT and LPT respectively. The bleed taken from B030 reenters via B041 after the Burner element.

The outlet flow from CmpH enters the burner element via B030, where the flow is mixed with the fuel stream provided by the FuelStart element, FusPri. After combustion, the hot gases are expanded by the two Turbine elements, the HPT TrbH and the LPT TrbL. The HPT and LPT power the HPC and fan respectively via the Shaft elements ShH and ShL.

The gas stream then enters the Mixer element, MixExh, where it is mixed with the bypass flow entering via D130. The inlet area of the Mixer element is set to be first calculated for the primary (core) stream, as it is slightly larger than the bypass stream.

Via the duct D060, the gas stream enters the second Burner element, BrnAug, which is the afterburner. The gas stream is mixed again with new fuel coming from the FuelStart element FusAug, where after the the stream enters and is expanded to ambient conditions in the nozzle, NozMix. Finally, the model flow is terminated when the stream out of the nozzle enters the FlowEnd element, after which the engine performance and cycle calculations are conducted by the EngPerf and Cycle elements respectively.

Below in Table 2. follows design data, e.g pressure ratios and pressure losses for some of the elements in the base model. The isentropic efficiency, η_{is} is also shown. The efficiencies have been gathered from the book *Elements of Propulsion, Gas Turbines and Rockets 2nd Edition*, which lists polytropic efficiencies, η_{pol}, (recalculated into η_{is} for the models), maximum temperatures etc. for the main components of aircraft engines. The values are given depending on so called "technology levels". For example, an efficiency given for technology level 3, TL3, corresponds to what is typical for aircraft engines from the period of 1985 - 2005 [5]. The TL3 values are what will be primarily used for the models in this thesis given that this is applicable to the bulk of the world's aircraft currently in service. A short look at how a switch to TL4 (2005 and forward) would affect the performance of the engine models will however also be taken later.

The equations used for recalculating polytropic efficiencies into isentropic efficiencies are for the compressor elements

$$\eta_{is} = \frac{\pi_c^{(\gamma-1)/\gamma} - 1}{\pi_c^{(\gamma-1)/\gamma * \eta_{pol}} - 1} \tag{8}$$

where γ is the heat capacity ratio of air (equal to 1.4) and π_c is the compressor pressure ratio. For the turbine elements, the corresponding equation is

$$\eta_{is} = \frac{1 - \pi_t^{(\gamma_{comb}-1)*\eta_{pol}/\gamma_{comb}}}{1 - \pi_t^{(\gamma_{comb}-1)/\gamma_{comb}}} \tag{9}$$

where γ_{comb} is the heat capacity ratio of the combustion gases (equal to 1.33) and π_t is the turbine pressure ratio.

Table 2: Some design data and efficiencies for the base model elements. Based on TL3 data.

Element	Design data	η_{is} [5]
SpltFan	BPR: 0.5	-
CmpFPri	PR: 4.0	0.8308
CmpFSec	PR: 4.5	0.8282
CmpH	PR: 8.0	0.8415
D025	-	-
D130	-	-
BrnPri	dP: 0.06 $T_{out,max}$: 1913 K [5]	0.99
TrbH	PR: 2.5 $T_{in,max}$: 1780 K [5]	0.8539
TrbL	PR: 1.9	0.8580
D060	-	-
BrnAug	dP: 0.06 [5]	0.94
NozMix	dP: 0.05	-

Some further things that are important for the design of the model are the fan pressure ratio, FPR, defined as

$$FPR = \frac{P_{fan,out}}{P_{fan,in}} \tag{10}$$

the engine pressure ratio, EPR, defined as

$$EPR = \frac{P_{LPT,out}}{P_{fan,in}} \tag{11}$$

and the mixer pressure ratio, PR_{mix},

$$PR_{mix} = \frac{P_{mixer,in,2}}{P_{mixer,in,1}} \tag{12}$$

where $P_{fan,out}$ and $P_{fan,in}$ are the total pressures of the streams in and out of the fan, $P_{LPT,out}$ is the total pressure going out of the low pressure turbine. $P_{mixer,in,2}$ and $P_{mixer,in,1}$ are the total pressures for the mixer inlets joining the bypass stream and core stream together respectively.

The engine needs to be designed in such a way that the fan outlet pressure is no more than 5 - 7 % higher than the LPT outlet pressure in order to minimize mixing losses [15]. Since the fan and LPT exit pressures must be similar, it thus follows that the FPR and EPR should be nearly equal to each other [15]. The base model has an FPR of 4.169 and an EPR of 4.286 in design mode - a difference of 2.8 %.

PR_{mix} is important to keep at a value above, and preferably close to 1. Otherwise, there may be a risk for some of the flow in the main stream to travel backwards through the duct with the lower pressure.

Deciding on different component design data to get a properly working model is largely an iterative process. Some input and target values, for example the EPR, are rather standard while others involve guess work. For example, the design BPR and compressor pressure ratios among others

have to be determined via educated guesses, whereafter the model is run to make sure the resulting component pressures, flows, Mach numbers etc., are reasonable.

2.4 Control of The Model

Below is described how the model is controlled.

2.4.1 General Control

Figure 4 below describes, in general, how the design/off-design mode and the afterburner model in the model are controlled. The flowchart is not all encompassing, neither with regard to the specific control sequences depicted nor the existing control sequences in general, but should provide an overview and general understanding of how the model functions when run.

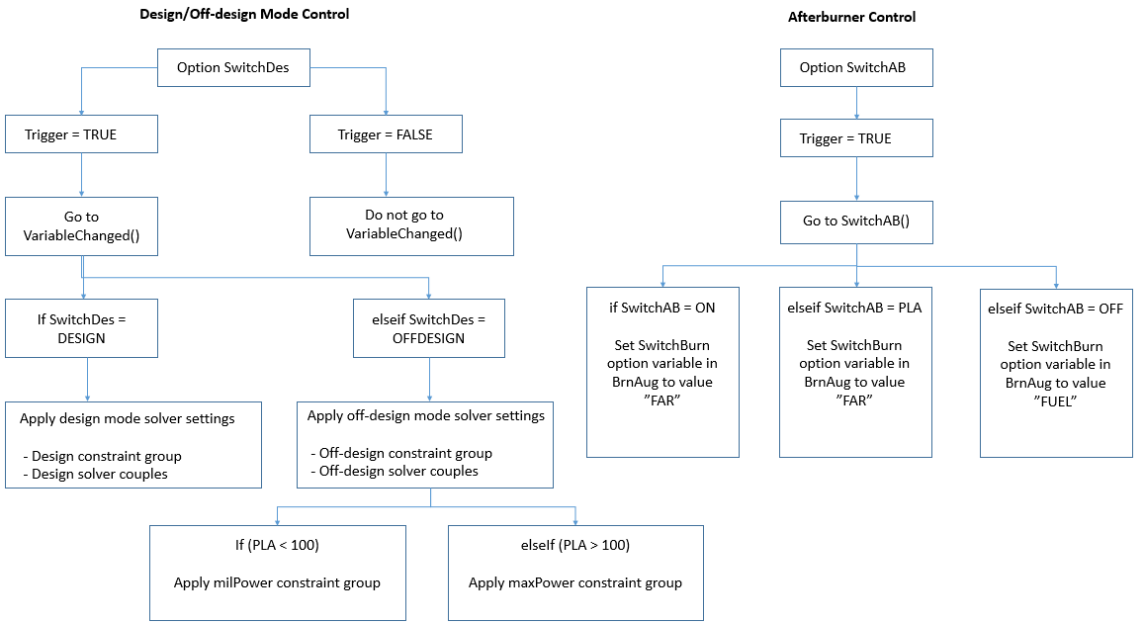

Figure 4: Flowchart of the general control of the model

The leftmost control sequence describes what follows when the value for the SwitchDes option variable is set. The option variable has a trigger, which if "FALSE", does nothing. If the trigger is "TRUE", the VariableChanged() function is used to determine whether the model has been set to either design or off-design mode. Depending on which mode is specified, the respective solver couples and constraints are set up. In off-design mode, these constraint groups are divided into either military power (dry thrust) or max power (wet thrust) constraints depending on the PLA value.

On the right hand side, there is the control sequence for the afterburner. If the trigger for the option variable SwitchAB is "TRUE", the SwitchAB() function is used to determine how the afterburner is controlled. In design mode, SwitchAB is set to "ON" and in turn, the option variable SwitchBurn inherent to the Burner element is given the value "FAR". When given this value, the burner/afterburner is set to uphold a specified fuel to air ratio. This results in the fuel flow coming from the fuel station (FusAug in this case) being set according to the air flow and fuel to air ratio [14]. If SwitchAB is set to PLA, which is the case during off-design runs, the given value will again be "FAR". In the case of this model, the fuel to air ratio is in turn determined by the PLA value.

Finally, if the SwitchAB option variable is set to "OFF", SwitchBurn is given the value "FUEL". This means that the afterburner will instead use a fuel input value provided by the user, and ignore whatever is provided by the fuel station (FusAug).

2.4.2 Model Solver Settings

Below follow some of (less interesting ones were omitted) the solver settings for the base model, beginning with the model constraints which set the maximum values for some engine parameters during any simulation. The constraints are divided into two groups: one for dry thrust settings and one for wet thrust settings.

- Dry thrust constraints:
  Max turbine inlet temperature (K)
  Max high pressure spool speed (%)
  Max relative corrected high pressure spool speed (%)
  Max relative corrected low pressure spool speed (%)
- Wet thrust constraints:
  Max turbine inlet temperature (K)
  Max relative high pressure spool speed (%)
  Max relative low pressure spool speed (%)
  Max relative corrected high pressure spool speed (%)
  Max relative corrected low pressure spool speed (%)

Following the constraints, there are naturally also the independent and dependent variable solver couples. Apart from those inherent to the elements themselves, there are some that are instantiated in the solver settings to control things such as BPR, pressure ratio etc. These solver couples, i.e. an independent variable and its corresponding dependent variable, are divided into two groups as well - one for design mode and one for off-design mode.

- Design mode solver couples:
  Independent: Bypass Ratio
  Dependent: Mixer Pressure Ratio

  Independent: Burner fuel flow (kg/s)
  Dependent: Target burner outlet temperature (K)

- Off-design mode solver couples:
  Independent: Burner fuel flow (kg/s)
  Dependent: Target burner outlet temperature (K)

  Independent: Nozzle outlet area (m^2)
  Dependent: Target fan stall margin rotational speed (rpm)

In design mode, the solver thus iterates the bypass ratio and burner fuel input until the specified mixer pressure ratio and the target burner outlet temperature are obtained respectively. In off-design mode, the solver also varies the outlet area of the nozzle until a specified rotational speed of

the fan is met. Though not technically part of the solver settings, it should also be pointed out that the BPR of the engine is set to the design BPR specified in the splitter element, BPRdes, during design mode. In off-design, the solver varies the BPR to meet a mixer pressure balance.

2.5 Design of VCE Models

It was decided to model not only one, but two VCE models with somewhat different design choices regarding BPR and some component design data. Going forward, these models will be referred to as design 1 and design 2. As for the overall model layout, they are the same. A schematic of the VCE model structure is presented in Figure 5 below.

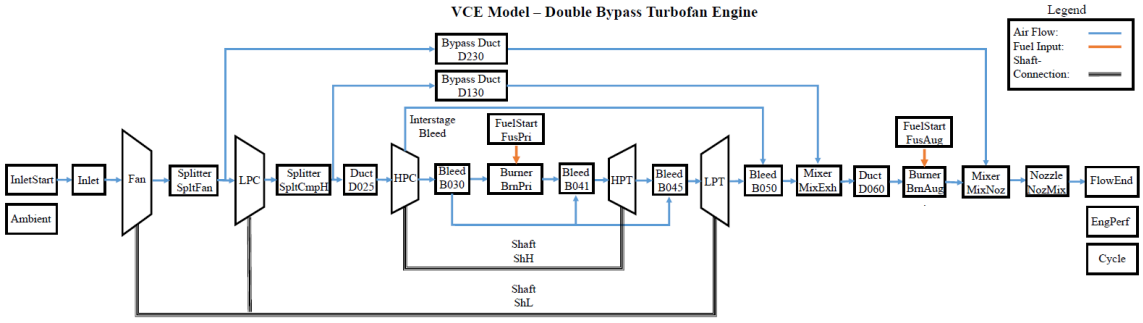

Figure 5: Flowchart of VCE Models (design 1 and 2)

The first difference to be seen between the VCE and base model layouts is that the VCE has only one fan section, with the splitter placed after it instead of before it. This decision was made in order to reduce the complexity of the NPSS code and make convergence easier when running the models. In order to still include the difference in enthalpy between the hub and tip sections of the fan and also the newly added LPC, a modified Splitter element has been used for the VCEs. This modified Splitter has an additional function included within it which takes a pressure increase as user input and calculates the corresponding temperature change, and the resulting enthalpy change. This enthalpy change is applied to the second outlet stream, i.e. the bypass stream. The equation added to the Splitter element to calculate the temperature change is the equation for isentropic compression of gases

$$T_{out} = T_{in} + \frac{1}{\eta_{fan,is}} * T_{in} * \left(\frac{P_{out}}{P_{in}}^{\frac{\gamma_{air}-1}{\gamma_{air}}} - 1\right) \tag{13}$$

where $\eta_{fan,is}$ is the fan isentropic efficiency, and T_{out}, T_{in}, P_{out} and P_{in} are the total temperatures and pressures for the stream entering and exiting the Splitter element. Since this equation assumes isentropic compression of the air, it is worth noting that the result will not be entirely exact. Using the isentropic efficiency rather than the polytropic efficiency to calculate the enthalpy change was decided upon for the sake of simplicity. While not ideal, it should nonetheless suffice for this project.

Exiting the first Splitter element, SpltFan, the flow is divided between the core stream and the outer bypass stream. The bypass ratio for this splitter will henceforth be referred to as the outer bypass ratio, or OBPR. The outer bypass stream goes to the outer bypass duct, D230, while the core stream continues to the low pressure compressor, the LPC. The LPC is attached to the same shaft as the fan, thus being a fan driven core stage (FDCS). The reason for adding the FDCS to the model is to allow for the pressures of the two bypass streams to be controlled separately from one another, which is important for the engine model to work as desired.

Exiting the LPC, the core stream enters a second Splitter element, SpltCmpH. As with SpltFan, this is a modified version of the Splitter element which raises the pressure and enthalpy of the second outlet stream. The second outlet stream going to the duct D130 is the inner bypass stream, and the bypass ratio of SpltCmpH is thus called the inner bypass ratio, or IBPR.

Continuing onward through the model layout, nothing has changed compared to the base model until arriving at a Mixer element, MixExh. The decision was made to design the VCEs as entirely mixed flow engines, i.e joining the the core stream and the bypass streams together before the exhaust through the nozzle. With two bypass flows, two Mixer elements are required to recombine all streams into a single stream. The existence of two mixing stages adds significant complexity to the engine due to the additional PR_{mix} that must be balanced, and is possibly the foremost source of challenges that comes with the design of this type of VCE. Despite the aforementioned problems that are inherent to such a design choice, it makes the most sense to configure the engine in this way. Including one or more separate nozzles for the bypass streams would, as explained in the theory on VCEs, possibly render the real engine impractical due to the added complexity and weight [3]. A mixed flow configuration is therefore likely a suitable choice in order for the model to have a higher chance to resemble something achievable in reality.

The core stream and the inner bypass flow are joined together in MixExh, where after the stream enters the afterburner. Exiting the afterburner, the flow enters the second Mixer element, MixNoz, before finally leaving the engine via the nozzle. This decision, to implement the second mixing stage after the afterburner rather than before it, warrants some clarification. From a pure engine thrust standpoint, this would be a suboptimal choice as the cold bypass air re-entering the stream would decrease the kinetic energy in the jet stream being propelled through the nozzle. Since the third stream is primarily being utilized during dry thrust, with comparatively little air passing through it during wet thrust, the effects of this configuration choice on thrust should however not be too detrimental. The rational design choice would nonetheless appear to be to instead mix the air before the afterburner stage as to maximize the thrust generated - particularly when operating wet. There are however a couple of reasons for designing the engine like this, with the first being to provide some cooling to the outward afterburner casing. The second reason is one of reduced thermal visibility; the exhaust plume of the engine produces a very high infrared signature that can be reduced by injecting cool air into the exhaust flow [16]. Given that the type of engine that this thesis deals with could likely be designed with stealth aircraft in mind, this design choice may not be that far-fetched and was deemed worthy of trying out.

As with the previous section on the base model, below follows some design data for the two VCE-designs in Table 3.

Table 3: Some design data and efficiencies for the VCE model elements.

Element	Design data - design 1	η_{is} - design 1 [5]	Design data - design 2	η_{is} - design 2 [5]
SpltFan	OBPR: 0.065	-	OBPR: 0.4	-
SpltCmpH	IBPR: 0.3	-	IBPR: 0.4	-
CmpFan	PR: 3	0.837	PR: 3.15	0.837
CmpL	PR: 1.2	0.877	PR: 1.2	0.877
CmpH	PR: 7.8	0.842	7.5	0.842
D025	-	-	-	-
D130	-	-	-	-
BrnPri	dP: 0.06 $T_{out,max}$: 1913 K [5]	0.99	dP: 0.06 $T_{out,max}$: 1913 K [5]	0.99
TrbH	PR: 2.5 $T_{in,max}$: 1780 K [5]	0.8539	PR: 2.5 $T_{in,max}$: 1780 K [5]	0.8539
TrbL	PR: 1.9	0.858	PR: 1.9	0.858
D060	-	-	-	-
BrnAug	dP: 0.06 [5]	0.94	dP: 0.06	0.94
NozMix	dP: 0.05	-	dP: 0.05	-

For the sake of a quick comparison between the different component efficiencies of the base model and VCEs (this will be relevant later), these are summarized below in Table 4 below.

Table 4: Component efficiencies for the different models summarized.

Element	η_{is} - base model (TL3/TL4) [5]	η_{is} - design 1 (TL3/TL4) [5]	η_{is} - design 2 (TL3/TL4) [5]
CmpFPri	0.8308/0.8669	-	-
CmpFSec	0.8282/0.8649	-	-
CmpFan	-	0.837/0.868	0.837/0.868
CmpL	-	0.877/0.897	0.877/0.897
CmpH	0.8415/0.8678	0.842/0.868	0.842/0.868
BrnPri	0.990/0.995	0.990/0.995	0.990/0.995
TrbH	0.8539/0.8769	0.8539/0.8769	0.8539/0.8769
TrbL	0.8580/0.8784	0.858/0.8784	0.858/0.8784
BrnAug	0.94/0.97	0.94/0.97	0.94/0.97

Other than the efficiencies, pressure drops and maximum temperatures are also affected by the switch to technology level 4. For all models, dP in the elements BrnPri, BrnAug and NozMix decrease from 0.06, 0.06, and 0.05 to 0.04, 0.05 and 0.02 respectively [5]. For the elements BrnPri and TrbH, $T_{out,max}$ and $T_{in,max}$ increase from 1913 K and 1780 K to 2135 K and 2000 K respectively [5].

2.6 Control of the Models

Below is described the control of the VCE models. The general control of the model, e.g. design/off-design mode and afterburner control remain the same as in the base model.

2.6.1 Control of Bypass Flows

As it is deemed crucial for a VCE to be practical in reality, an attempt was made to model a VABI element, inserting one each at the mixing planes of the bypass and core streams. The VABI element was based on a Valve element which is a standard element in NPSS. To create the VABI, the Valve element was modified to have its output area controlled by a control schedule. The idea was to have the control schedule specify the BPR of the engine depending on the power setting, which in turn would correspond to a value determining the percentage of the VABI being open. For example, at max power settings, the control schedule would specify the minimum BPR that the engine would operate at with the outer VABI closing off most of the airflow to maintain the pressure balance. In practice, this approach to modelling a VABI proved to be fundamentally flawed and very difficult to get to a working state. Convergence issues while running the simulations due to the elements not being able to operate at the conditions stemming from the specified bypass ratios were frequent. If convergence somehow was achieved, the performance was similar or worse than what was obtained from letting the NPSS solver calculate the airflow on its own. The futility in trying to manually specify some optimum BPR for each possible operating point of the engine was soon realized. If a VABI is to be modelled, some other more complicated design approach is needed. A possible solution could perhaps be to instead control the fan air intake, with the VABI elements adjusting their outlet areas to balance the mixing plane pressures as the flows through the different ducts shift. Due to the time constraint of this project, modelling a working VABI element unfortunately had to be abandoned.

2.6.2 Model Solver Settings

The model solver settings for the VCEs are similar to those of the base model. For the sake of clarity, these will also be listed below. First follow the constraints, which are identical.

- Dry thrust constraints:
  Max turbine inlet temperature (K)
  Max high pressure spool speed (%)
  Max relative corrected high pressure spool speed (%)
  Max relative corrected low pressure spool speed (%)
- Wet thrust constraints:
  Max turbine inlet temperature (K)
  Max relative high pressure spool speed (%)
  Max relative low pressure spool speed (%)
  Max relative corrected high pressure spool speed (%)

  Max relative corrected low pressure spool speed (%)

Following the constraints, there are again the independent and dependent variable solver couples. These differ somewhat between the two VCE designs.

- Design mode solver couples - design 1:
  Independent: Inner Bypass Ratio
  Dependent: Mixer (MixExh) Pressure Ratio

  Independent: Burner fuel flow (kg/s)
  Dependent: Target burner outlet temperature (K)

- Design mode solver couples - design 2:

  Independent: Burner fuel flow (kg/s)
  Dependent: Target burner outlet temperature (K)

- Off-design mode solver couples - designs 1 and 2:
  Independent: Burner fuel flow (kg/s)
  Dependent: Target burner outlet temperature (K)

  Independent: Nozzle outlet area (m^2)
  Dependent: Target fan stall margin rotational speed (rpm)

For design 1, the solver couples are thus set up the same way as in in the base model. It only differs from the base model in that the BPR and mixer PR solver couple has been amended to reflect the difference in the models. The independent variable is now specifically the inner bypass ratio while the dependent variable is specifically the pressure ratio of the first mixer, MixExh. For the design 2 however, the solver does not iterate the IBPR to match the mixer PR. Doing this allows for both the IBPR and OBPR to be set to a design value in design mode. Though Table 2 and Table 3 both list a design value for the BPR/IBPR, these are in actuality only initial guesses for the solver to work with.

2.7 Model Evaluation

The VCE models were evaluated compared to the base model in three different ways. At first, the models were simulated with so called PLA sweeps, where the PLA is varied in the range of 50 to 150 at different altitudes and flight Mach numbers. PLA stands for Power Lever Angle, which is the angle of the pilot's throttle control lever. The higher the PLA value, the more thrust is produced by the engine. At a PLA of 50 for example, the throttle is situated at 50 ° angle and is the minimum amount of thrust that will be used in any simulation conducted for this thesis. Conversely, at a PLA value of 150 the throttle lever is positioned at 150 °, meaning that the engine is running at full power with the afterburner ignited. The PLA threshold for going from dry to wet thrust is at a value of 100.

2.7.1 PLA sweeps - Varying Mach and Altitude

To begin with, PLA sweeps were conducted at what would constitute the conditions in a stationary engine test rig, so called SLS (Sea Level Static) i.e. Mach and altitude being both at 0. Thereafter, PLA sweeps were conducted at altitudes of 30 000 and 15 000 ft. at four different flight Mach numbers. The results of interest in this case were the variations of SFC, F_n and the different bypass ratios. In addition to the IBPR and OBPR, the results shown also include the total bypass ratio, or TBPR, for the VCE designs. For the base model, there is no difference between the TBPR and the BPR. The TBPR is defined as

$$TBPR = \frac{\dot{m}_{230} + \dot{m}_{130}}{\dot{m}_{025}} \tag{14}$$

where $\dot{m}_{230}$, $\dot{m}_{130}$ and $\dot{m}_{025}$ are the air flows through the ducts D230, D130 and D025 respectively.

2.7.2 Two-parameter Sweeps at Constant PLA - Creation of Level Plots

The behaviours of the VCEs compared to the base model was also visualised by running two-parameter sweeps at constant PLA, where both the altitude and inlet flight Mach numbers were varied throughout their respective ranges - 0 to 40 000 feet and Mach 0 to Mach 1.8. The PLA was first set at max dry thrust, i.e. 99, but had to be lowered to 90 since convergence problems started occurring when setting the throttle close to the afterburner threshold of 100. The result of these sweeps are very detailed level plots, where the performance at every point within the specified Mach number and altitude ranges can be seen. This time, the only performance parameter plotted was the SFC.

2.7.3 Mission Analysis

This sections explains the perhaps most interesting segment of the model evaluations - the mission analyses. The basis for the mission analysis has been gathered from the publicly available *Standard Practice Glossary of Definitions, Ground Rules, And Mission Profiles to Define Air Vehicle Performance Capability* published by the US Department of Defense [17], as well as the chapter on mission analysis from the book *Aircraft Engine Design* [18]. The first document presents in its appendix different mission profiles for air vehicles, whose explicit purpose is to lay out a structure for the comparison of performance and capability between different aircraft conducting the same mission [17]. The document specifies times and/or distances for different segments of the mission, with exception for some portions which are left blank since this "provides the variability needed to maximize the parameter of interest" [2, p. 67]. Since the VCEs modelled in this thesis are intended for use in military aircraft, the basis for the mission constructed for this thesis is a military one. More specifically, the Combat Air Patrol (CAP) mission profile [17]. The justification behind using this particular mission profile as a basis is the inclusion of significant portions of loitering, i.e. flying at high altitude at low velocity where the VCE is likely to have produce the largest improvement to performance. The altered mission used in the thesis has been simplified and limited somewhat to exclude the segments where the aircraft operates at supersonic speeds however. The analysis conducted for this thesis is further limited to the performance in terms of the total amount of fuel consumed during the mission sweep. Below in Figure 6, a schematic of the mission used is shown.

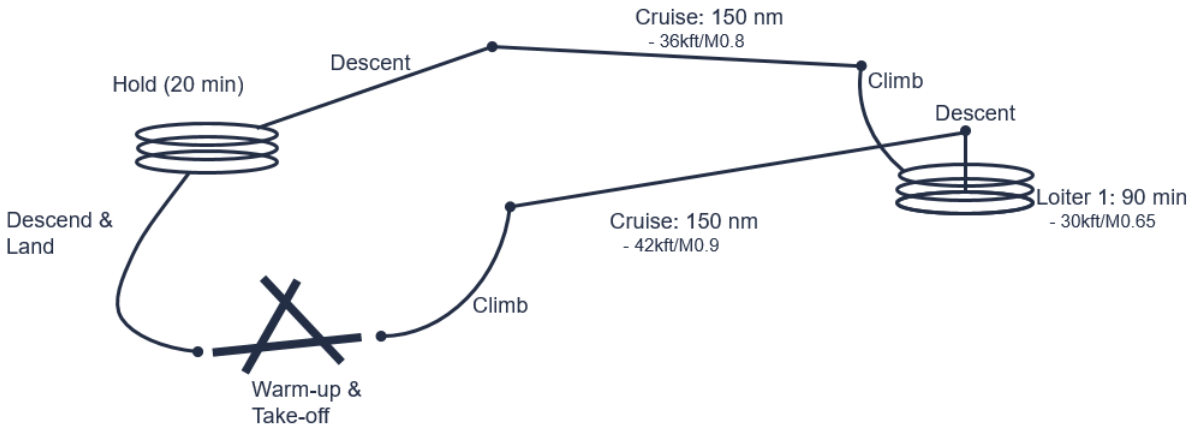

Figure 6: Schematic of Mission Segments

The mission naturally begins with the aircraft warming up its engines lower thrust settings before take-off, before it accelerates to maximum power and lifts from the ground. This portion has been omitted from the calculations for simplicity's sake, since the time spent at this segment is very short

compared to the rest of the mission. Next, the aircraft begins its climb up to 42 000 ft. where it operates at maximum wet thrust. Apart from the climb itself, the aircraft also travels a distance of 20 nautical miles during this segment. Both the inlet air conditions and aircraft velocity will naturally both vary during a climb, which needs to be taken into account when running the mission sweep in NPSS. Thankfully, the mission example in [14] provides flight Mach numbers at several points during this climb, which can be used as a basis for the points simulated in the mission sweep. The Mach numbers increase from 0.7 to 0.9 during the climb, where Mach 0.9 is reached already at 30 000 ft. The rest of the climb is made at constant velocity. This portion of the mission will be used as a showcase for how the total fuel consumption is calculated for the mission.

The climb up to 30 000 ft. is divided into 8 sections, where the velocity is assumed to increase linearly from Mach 0.7 to Mach 0.9. The distance taken into account is the total distance travelled vertically as well as horizontally (the diagonal in the triangle formed with the vertical and horizontal changes as each catheter). For each segment, the time needed to make the climb is calculated by dividing the total travel distance by the velocity of the segment. Though the velocity would in reality of course continually increase throughout each individual segment, the velocity used for each segment is, for simplicity's sake, the initial velocity of each segment. The remainder of the climb up to 42 000 ft., which now takes place at a constant velocity of Mach 0.9, is divided into 4 segments with the time for each segment calculated in the same manner as before. With the duration of each segment now defined, and the SFC at each segment known from the results output, the total fuel consumption is easily calculated. After the initial climb, the throttle is pulled back to a PLA of 90 and the aircraft cruises for 150 nautical miles at the altitude 42 000 ft. and at a Mach number of 0.9. This is performed as one single mission segment in NPSS. It thereafter descends to 30 000 ft. (omitted from the mission sweep) where it loiters for 90 minutes at Mach 0.65 and PLA = 70. The aircraft then performs its second climb up to 36 000 ft. with the throttle back to a PLA of 90, increasing its speed from Mach 0.65 to Mach 0.8. It now conducts its second cruise at Mach 0.8 and PLA at 90. From there, it descends to 15 000 ft. (omitted from the mission sweep) where it loiters for another 20 minutes at Mach 0.6 and PLA at 60. Lastly, the aircraft makes its final descent and landing (omitted from the mission sweep).

3 Results

3.1 Sea Level Static Performance

The results for the PLA sweeps at SLS conditions are presented below. The results for both SFC and F_n are presented in Figure 7 and are shown as percentages of what the base-model achieved, while the bypass ratios (TBPR, OBPR, IBPR), of all models presented in Figure 8 are shown with their actual values.

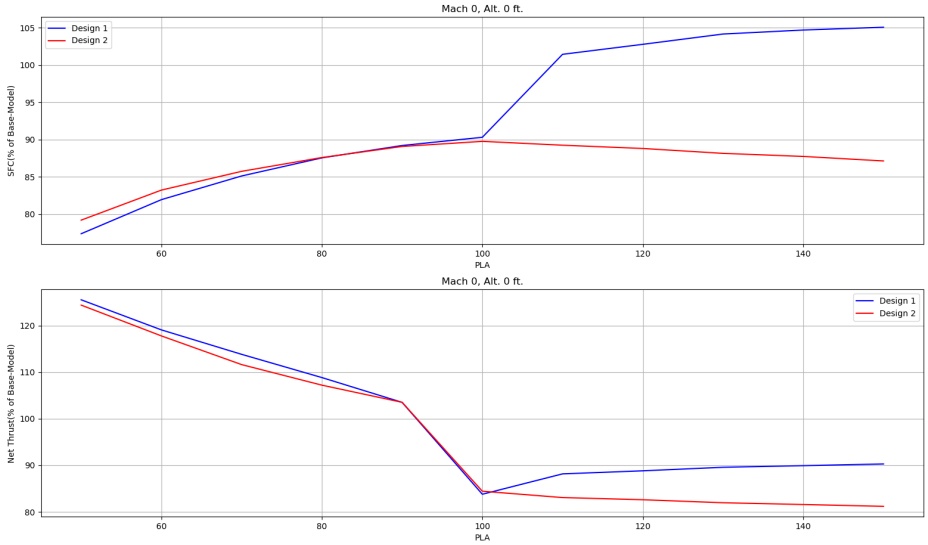

Figure 7: SFC and F_n for designs 1 and 2 at Mach 0 and altitude 0 ft.

The results for both SFC and F_n are very similar in the dry-thrust region (PLA $<$ 100 - afterburner not started), above which they begin to greatly differ once the afterburner has been started. At the lowest throttle, the SFC of designs 1 and 2 respectively is ca. 21 and 23% lower than for the base-model while the net thrust is around 26 and 25 % higher. Design 1 has better SFC than the base-model up until PLA goes into the wet thrust (afterburner turned on) region, after which it rapidly increases compared to the base-model. For design 2, the SFC is comfortably below the one of the base-model for the entire sweep, even increasing the gap in the wet-thrust region.

The net thrust, F_n, goes below that of the base-model around a PLA of 90. For design 1, the SFC at the design point of PLA = 150 is ca 5% higher than that of the base-model, while the SFC of design 2 is ca. 13% lower. Design 2 could thus be seen as superior regarding savings of SFC with the afterburner on, but it comes at the cost of a ca. 18 % drop in net thrust at maximum throttle. Design 1, while not saving the same amount of fuel as design 2, still retains ca. 90 % of the maximum F_n achieved by the base model.

The behaviour of the bypass ratios for the base model and VCEs at SLS conditions can be seen in Figure 8 below.

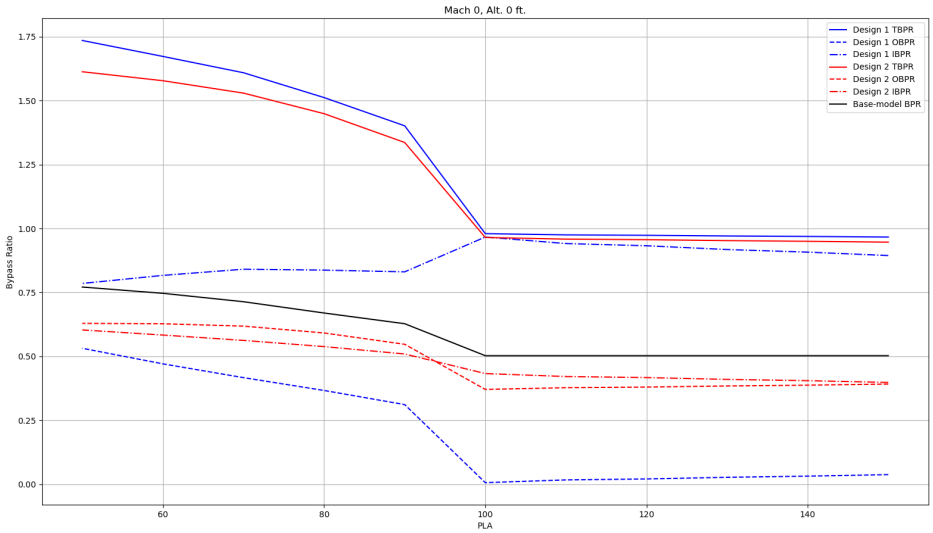

Figure 8: TBPR, OBPR and IBPR for VCE designs and base-model at Mach 0, Alt. 0 ft. and varied PLA.

The TBPR is somewhat similar between the two VCEs throughout the PLA sweep, as well as significantly higher than for the base model. At minimum PLA, the TBPR is around 1.74 and 1.61 for designs 1 and 2 respectively, while being ca. 0.77 for the base-model. As PLA increases and the afterburner is turned on however, the TBPR does not fall below 0.95 for any of the VCEs in contrast to the base-model whose BPR approaches 0.5. This concurs with the SFC- and F_n-charts in Figure 7 which showed improvements to the SFC and F_n for the VCEs at low PLA at the cost of lower F_n at high PLA.

Looking at the OBPR and IBPR, it can be established that they behave differently between the VCEs, as is to be expected given the design differences. For design 1, the OBPR is at its maximum at PLA = 50 where after it eventually sinks close to 0 as the PLA increases. The IBPR has much less variation, increasing until it reaches the wet-thrust region whereafter it decreases slightly, approximately remaining in the span of 0.8 - 0.95 for the entire sweep. For design 2, The OBPR and IBPR are somewhat alike throughout the sweep, with the OBPR having a sharper decrease between PLA 90 and 100, while the decrease for IBPR is more linear.

Design 2 clearly has a narrow range of both IBPR and OBPR for which acceptable pressure ratios in the mixers can be maintained, while this limitation only holds true for the inner BPR in design 1. The key difference between the BPRs for designs 1 and 2 can thus be summed up with the following statement: As PLA increases, the OBPR and IBPR for design 1 start to diverge greatly, with the former decreasing and the latter increasing. For design 2, the OBPR and IBPR maintain very similar values throughout the sweep.

3.2 Performance at Set Altitudes with Varying PLA

3.2.1 High Altitude

For this section, the results for how the two different engine designs measure up to the base model in terms of SFC and net thrust in flight at 30 000 ft., as well as how the bypass ratios behave for the models, are displayed. Below in Figure 9, the results are shown for the performance in terms of SFC for both designs. The SFC is again shown as a percentage of the base model's SFC, while

the bypass ratios are presented with their actual values. Take note that some points in the graphs should be taken with scrutiny, as they present rather infeasible real life conditions. For example, flying at supersonic speeds above Mach 1 while being at part power with the PLA below 100 is not very realistic, and could at most represent a brief point in time where the throttle is pulled back when already moving at high velocity.

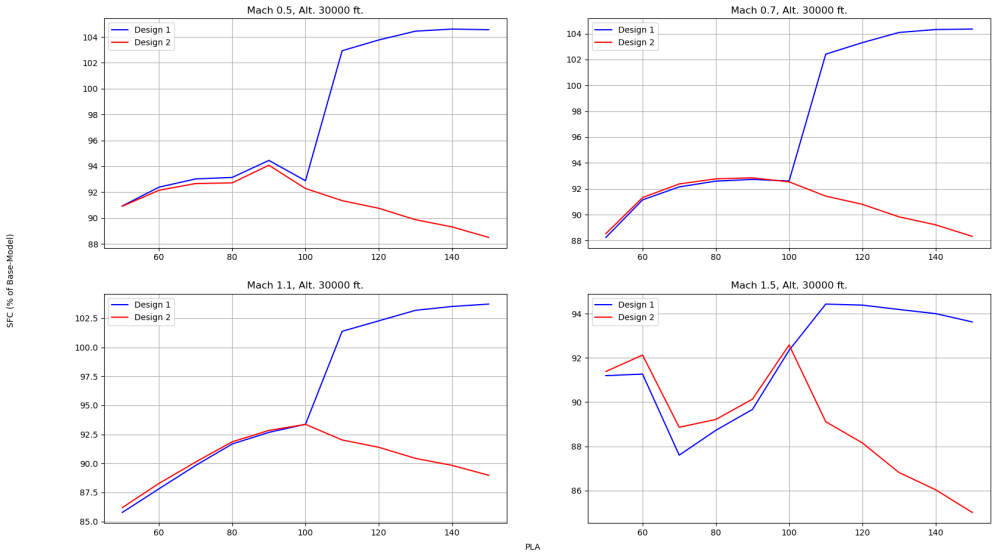

Figure 9: SFC for designs 1 and 2 compared to base model for varying PLA and Mach numbers at 30 000 ft.

The PLA sweeps were all done at the same altitude of 30 000 ft. The Mach numbers were not chosen with any particular consideration other than to represent a reasonable selection of different flight conditions, ranging from subsonic cruise flight at Mach 0.5 to supersonic flight at Mach 1.5. Particular import should however be placed on the results for Mach 0.7, as this flight Mach number at the given altitude is a fairly reasonable loitering condition, where the aircraft may spend much time during a mission (as is the case for the mission simulated further down). It can clearly be seen that both VCE designs represent a marked improvement to the SFC at dry thrust for all flight conditions, with the two designs achieving very similar results. Once PLA moves into the wet thrust region and the afterburner is ignited however, the results for the two designs begin to diverge. Design 1 has a rapid increase in SFC, which eventually overtakes the one of the base-model by barely 5 % at the most. The exception to this is seen at Mach 1.5, where the SFC remains appreciably below the one of the base-model for the entire sweep. The SFC curves now also form a dip like shape between PLAs 60 and 100, reaching their minimum at PLA = 70. The explanation for this can be found if one skips forward a bit to figures 10 and 11. There it can be seen that at Mach 1.5 and 30 000 ft., both the net thrust and total bypass ratio relative to the base model reach their peaks at a PLA of 70. Design 2 retains the decreased SFC compared to the base-model for the entire range of all four sweeps, even further increasing the gap between it and the two other models with the afterburner ignited. As could be previously seen in the SLS conditions shown in Figure 7, the second engine design seems to have the edge as far as fuel efficiency is concerned, if only with the afterburner running.

Again, the better SFC during wet-thrust for design 2 comes at the cost of decreased maximum F_n. Below in Figure 10, the results for the variation of F_n with PLA for the same sweeps can be seen. The value for F_n is presented as a percentage of the base-model's.

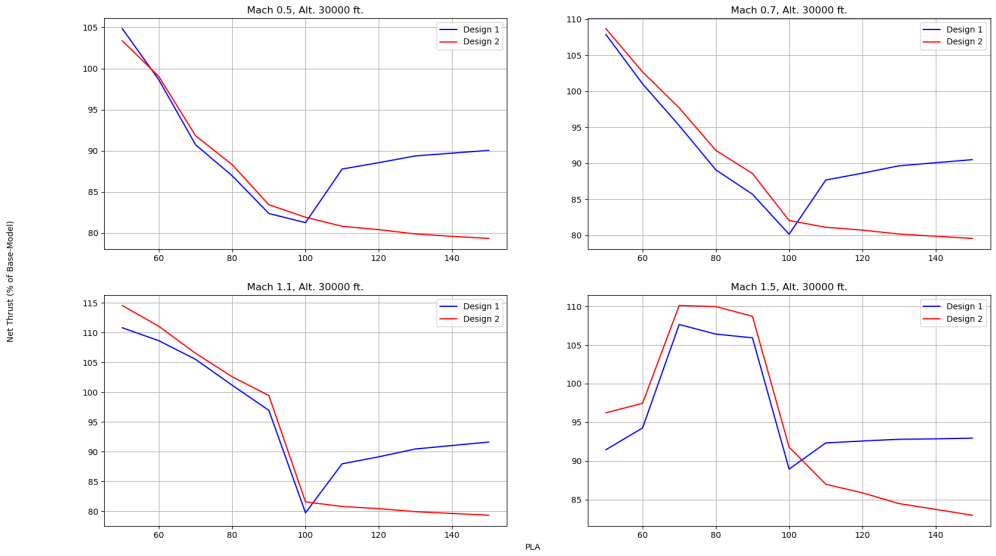

Figure 10: F_n for designs 1 and 2 compared to base model for varying PLA and flight Mach numbers at 30 000 ft.

From these results, it can be seen that both VCEs have an advantage over the base-model in the lower range of the dry-thrust region for the first three conditions, the results behaving differently at Mach 1.5, with the breaking point seemingly lying in the 60 - 90 PLA range depending on the flight condition. For the lowest PLA, the F_n achieved by the VCEs is between around 3 - 5 % higher than the base model's at Mach 0.5, barely 7 - 8 % higher at Mach 0.7 and 10 - 15 % higher at Mach 1.1 with design 2 having the edge. At Mach 1.5, the VCE designs appear to perform at their best in the PLA range of 65 - 95, peaking at little more than a 10 % thrust increase for design 2, and 7.5 % for design 1.

Moving on to the results for the engines running at wet-thrust, we see the cost of the increased fuel efficiency for both VCEs as the maximum achievable F_n is negatively impacted. This is particularly true for design 2, which has as much as 20 % lower F_n than the base-model at maximum throttle. Design 1 fares better in this case, managing to maintain above 90 % of the F_n compared to the base model at full throttle.

For the bypass ratios of the models, the results can be seen below in Figure 11.

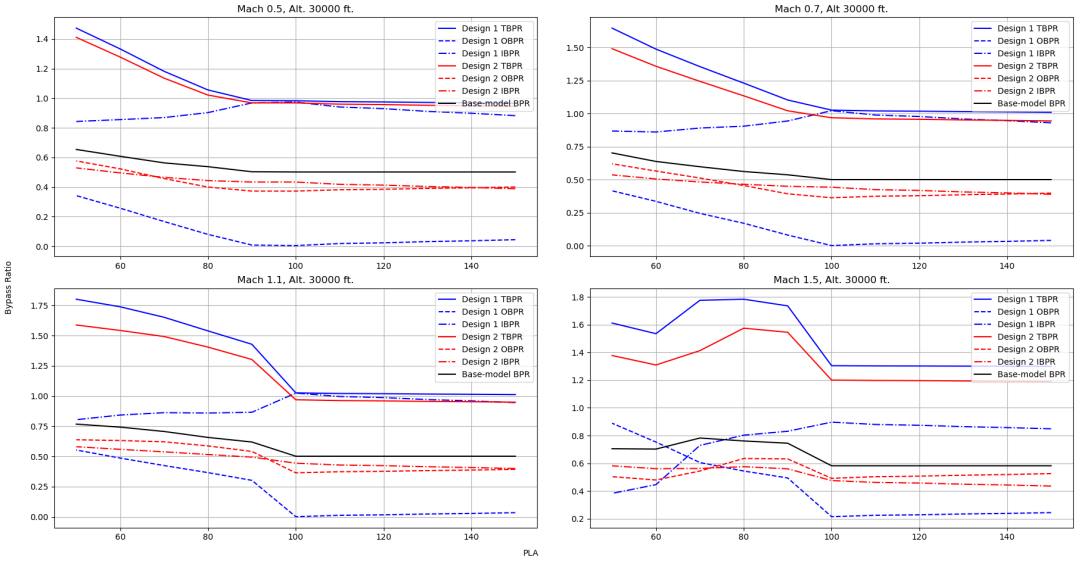

Figure 11: TBPR, OBPR and IBPR for VCE-designs and base-model for varying Mach numbers at 30 000 ft.

At Mach 0.5, 0.7 and 1.1, nothing really stands out compared to the SLS results in Figure 8. The patterns for the different bypass-ratios are rather similar, with the absolute values differing slightly and with the TBPR for design 1 being consistently higher than the TBPR for design 2. A trend that can be seen is that as the Mach number increases, so does the TBPR and OBPR at low PLA while the IBPR decreases slightly. At Mach 1.5 however, things become more interesting. Here, the TBPR curves for the VCEs as well as the base model do not decline steadily any more between PLAs 50 and 100, but rather form a crest like shape.

For design 1, the difference in IBPR between PLAs 50 and 100 is much more stark than before, increasing from under 0.4 to ca. 0.9. The OBPR also has a very large decline, starting at a very high 0.9 at PLA = 50, but no longer reaches 0 as before, instead settling at around 0.2 once the afterburner is ignited. This is easily explained by the fact that at such a large flight velocity, the air intake is too large to handle for the core and inner bypass stream alone any more, even with the engine at full power.

Finally, the key difference between the two VCE designs can be summed up in the same way as for the SLS conditions, with the OBPR and IBPR diverging greatly for design 1 while they remain very similar throughout the sweep for design 2. Observe also that at the lower PLA range for Mach 1.5, the IBPR for design 1 now starts at a lower value than the OBPR. The two BPRs eventually intersect at a PLA of ca. 65. It should now again be pointed out that any points below PLA of 100 at supersonic speeds, these included, should be viewed with skepticism. Nonetheless, for the brief moments that these points could theoretically exist, an explanation for what's observed here could be that the air flow through the core required by the engine is relatively low compared to the amount of air that will inevitably pass through at such a high flight speed.

3.2.2 Medium Altitude

In this section, the engine performance at a medium altitude of 15 000 ft. is presented. As with the high altitude performance, this will include the SFC, F_n and bypass ratios, where the SFC and F_n are again presented as a percentage of the corresponding results for the base-model. Beginning with Figure 12 below, the results for the SFC at Mach 0.5, 0.7, 1.1 and 1.5 are shown.

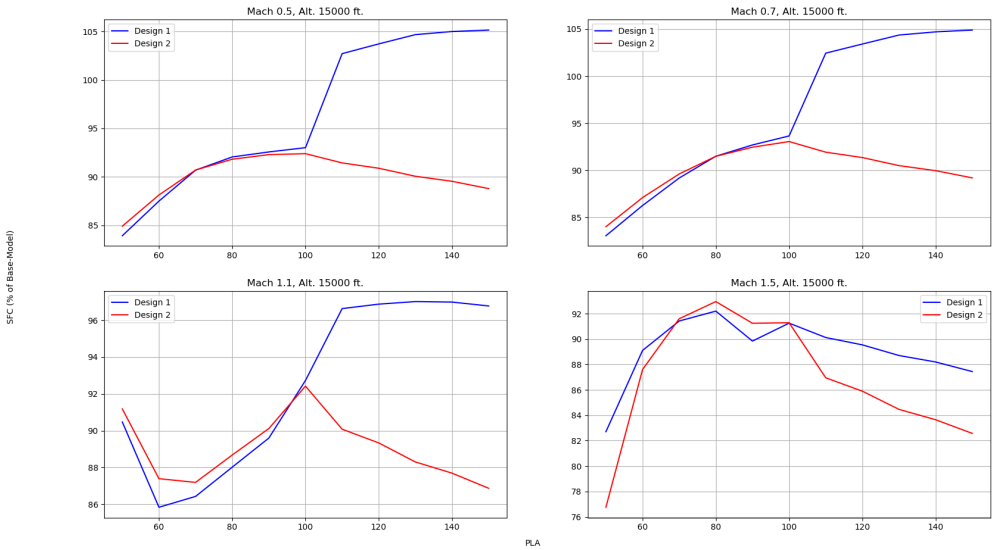

Figure 12: SFC for designs 1 and 2 compared to base model for varying PLA and Mach numbers at 15 000 ft.

The first thing to notice is that the performance of the VCEs compared to the base-model's is overall better at this altitude than at 30 000 ft. At Mach 0.5 and 0.7, the curve patterns are similar to those in Figure 9, with the primary difference being that the SFC reaches even lower levels at minimum PLA - ca. 15 and 16 % better than the base-model at Mach 0.5 and ca. 16 and 17 % better than the base-model at Mach 0.7 for designs 1 and 2 respectively.

The patterns for Mach 1.1 and Mach 1.5 at this altitude differ from the ones at 30 000 ft. At Mach 1.1, the minimum SFC can be found to be ca. 12.5 % and 14 % at PLA = 60 for designs 1 and 2 respectively, with the SFC never exceeding that of the base-model for any PLA. At Mach 1.5, the SFC is as much as 17 and 23 % lower at PLA = 50 for designs 1 and 2 respectively. The SFC peaks at around 92 % of the base-model SFC at PLA = 80 for both designs, somewhat steadily decreasing thereafter.

Arriving at the results for the development of F_n with PLA in Figure 13 below, we see some familiar patterns and some unfamiliar ones. The values for F_n are again shown as a percentage of the corresponding values of the base model.

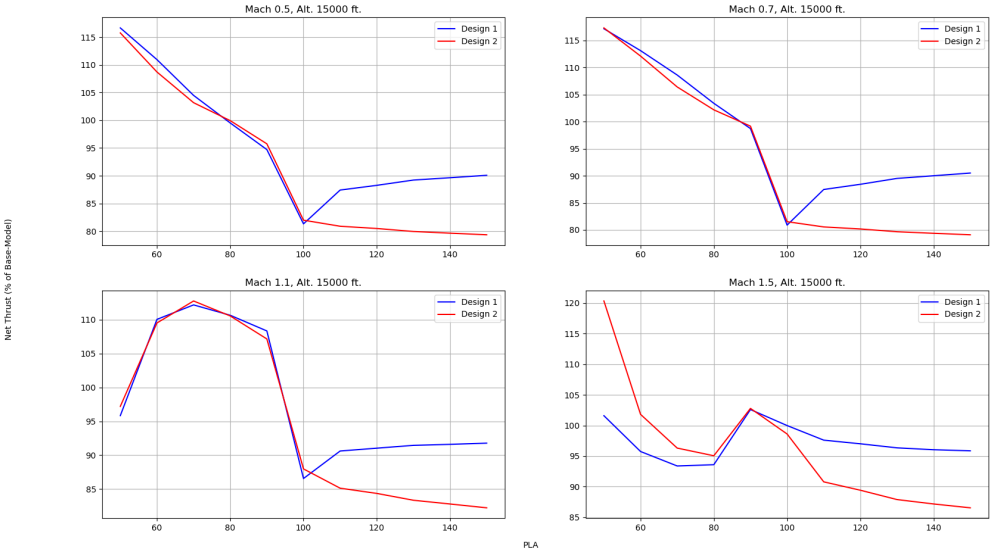

Figure 13: F_n for designs 1 and 2 compared to base model for varying PLA and Mach numbers at 15 000 ft.

As with the SFC, the results for F_n are overall better than at 30 000 ft. For Mach 0.5 and 0.7, the results for the net thrust produced by the VCEs in comparison to the base model during wet-thrust are very similar in both the curves' appearances and values to the results at 30 000 ft. F_n is however an entire 15 - 17 % higher at PLA = 50.

At Mach 1.1, F_n for the VCEs is lower than that of the base model at PLA = 50, but then rises sharply to its peak of an additional 13 %. At PLA = 150, F_n for design 1 is at 92 % of the base-model, which is slightly higher than it was at 30 000 ft.

Lastly, at Mach 1.5, The F_n-curves for the two VCEs differ greatly for the entire PLA sweep with the exception of PLA = 90 where they are practically the same. At PLA $<$ 90, design 2 has higher F_n with the peak being at ca. 20 % more than the base-model's. The peak for design 1 lies at PLA = 90. Moreover, it should be pointed out that at portions of the range of PLA below 90, the base model's net thrust exceeds one or both of the VCEs. Finally for Mach 1.5, design 1 reaches an entire 96 % of the net thrust produced by the base-model at PLA = 150, with the net thrust of design 2 sitting at ca. 87 % of the base-model's at the same point.

The behaviour of the bypass ratios for the different models at the Mach numbers and the altitude currently discussed is presented below in Figure 14.

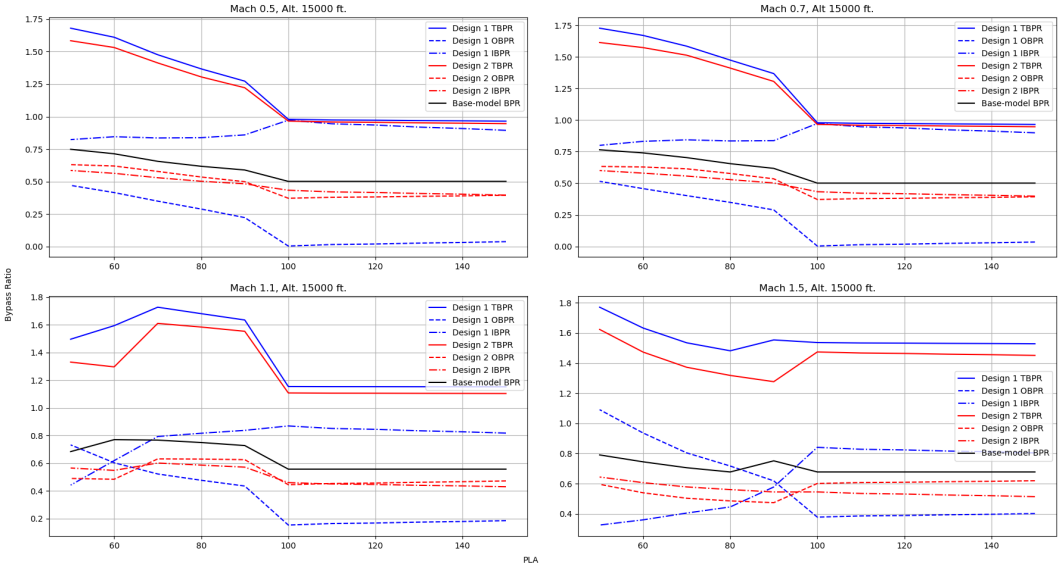

Figure 14: TBPR, OBPR and IBPR for VCE-designs and base model for varying Mach numbers at 15 000 ft.

As with the cases of the SLS conditions and the altitude of 30 000 ft., the TBPR of design 1 is higher than the TBPR for design 2 with both being very much higher than the base-model BPR. Furthermore, the bypass ratios at this altitude and Mach 0.5 and 0.7 are very similar the ones at the corresponding Mach numbers for 30 000 ft.

Some noticeable differences can begin to be seen at Mach 1.1 where the TBPRs for the VCEs no longer decrease between PLAs 50 and 100 in a linear fashion, instead forming a crest that peaks at PLA = 70. At PLA $\geq$ 100, the TBPRs are practically constant as they have been before, but their values now lie at a rather high 1.1 and above. The OBPR and IBPR for design 1 change significantly between PLAs 50 and 100, with the OBPR reaching a minimum of ca. 0.2 - something that did not occur until Mach 1.5 at 30 000 ft. The reason behind the OBPR being comparatively high at this altitude could be explained by the ambient pressure and air density being higher. The higher ambient pressure causes the pressure ratios and rpm values of the fan and compressors to be lower. This in turn means that the rpm values of the turbines will be lower as well, allowing less expansion in these stages to take place. When the flow thus reaches the final mixing stage, the core flow has a comparatively higher pressure, which necessitates a higher flow in the outer bypass channel. As to why the higher air density affects this is rather simple; a higher density means a higher mass flow intake and thus a larger proportion of the flow that must be redirected past the engine core.

At Mach 1.5, The TBPRs for both VCEs reach a minimum already in the dry-thrust region at PLA = 90, after which they increase and remain more or less constant at PLA = 100 and above. The magnitude of the TBPRs with the afterburner running are now very high around 1.55 and 1.45 for designs 1 and 2 respectively. The OBPR for design 1 reaches a value of 1.1 - its highest value yet for any of the sweeps conducted. The OBPR then decreases until PLA = 100, where it settles around 0.4 - also a very high value with the afterburner online. The values for the design 1 OBPR and IBPR now also intersect at a PLA of around 90 - a significantly higher PLA than they have intersected at in any of the other sweeps.

The key difference between the two VCEs seems to remain the same as at the previous sweep-conditions; the OBPR and IBPR of design 1 diverge greatly from one another while the OBPR and IBPR of design 2 remains rather alike throughout the PLA sweeps.

In summary, positive effects of the second bypass stream seem to be more noticeable at medium altitude than at high altitude. The subsonic improvement to SFC is greater while more of the maximum supersonic thrust is maintained compared to at high altitude.

3.3 Technology Level Impact

Below in Figure 15, the difference in terms of SFC that a switch to TL4 component specifications could entail can be seen. The graph shows the improvement for the base model and the first VCE model design in terms of SFC at different PLA and at SLS conditions compared to what was achieved with the TL3 component specifications. The second VCE design is not included as, unfortunately, running the model with the TL4 specifications returned negative Mach numbers in the bypass streams leading in to the two mixer elements - MixExh and MixNoz. As a quick reminder, the TL3 specifications represent component specifications between the years 1985 and 2005, while the TL4 specifications represent specifications from 2005 and onward.

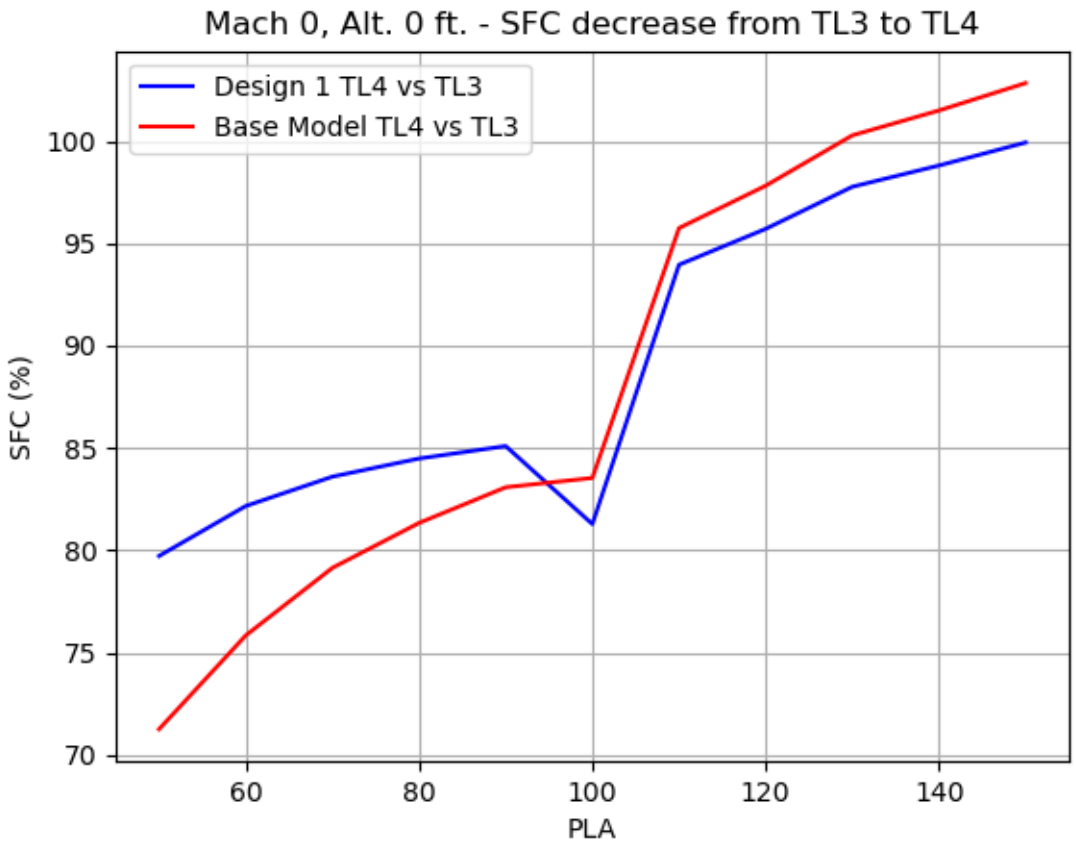

Figure 15: Percentage of SFC for base model and design 1 at TL4 compared to TL3 - SLS conditions.

The impact of such a switch is quite stark - particularly for the base model when operating at dry thrust. At full throttle, the difference is negligible for the VCE, but overall becomes increasingly larger the more the throttle is pulled back. The exception is the point where the afterburner is engaged at PLA = 100, where pulling the throttle back and shutting off the afterburner increases the SFC consumption compared to the model with TL3 component specifications. Though the dip between PLA 90 and 100 might seem odd at a first glance, there is a simple explanation. At PLA = 100, the afterburner is engaged, meaning that the model is controlled differently (different

constraints) than at PLA = 90. Had there been more points between the PLAs 90 and 100, the SFC would follow a more regular pattern up until a PLA of 99, after which the sudden drop would take place.

For both engine models, the largest impact of the upgrade of the components from TL3 to TL4 can be seen at the lower thrusts, with SFC rising rapidly in the wet thrust region. Comparing with the data in Table 4 in the methodology section, it's not entirely obvious what causes this since every element bar the primary burner sees a marked improvement to performance. Of the turbomachinery components however, the fan elements (CmpFPri, CmpFsec and CmpFan) see the largest improvements to efficiency. The lower the PLA, the less air flow is directed through the inner bypass channel and the engine core, meaning that the work provided by the LPC, HPC, LPT and LPT is decreased. The impact that the efficiency improvement in these elements has on the SFC is thus lessened at the lowest thrusts, in contrast to the fans which are always working with 100 % of the airflow taken into the engine.

The difference between how much the SFC of the two engine models is improved is also rather large. At a PLA of 50, the technology level upgrade has resulted in a difference in SFC improvement of ca. 8 % points between the two models. In part, this could be explained by the larger improvement to efficiency seen in the fan elements of the base model (CmpFPri and CmpFSec) compared to the fan element in the VCE model (CmpFan). Looking into the simulation results files however, some further interesting observations can be seen. For both models, the bypass ratios increase significantly at PLA 50 when increasing the technology level. The increases are from ca. 0.77 to 2.08 for the base model and from ca. 1.75 to 3.56 (OBPR) for the VCE. Percentage wise, the base model has seen the largest improvement in this regard, which would explain the larger SFC improvement as well. These much increased bypass ratios in turn seem to be caused by the decreased fuel and air demand of the burner, which can be attributed to the improved performance of the individual components - in particular the maximum in- and outlet temperatures of the HPT.

The afterburner element, BrnAug, has also had a large improvement to its combustion efficiency with the technology level switch, but this evidently does not seem to matter too much given the sharp rise in SFC in the wet thrust region. This should come as no surprise, as the afterburner consumes far more fuel than the primary burner. At maximum thrust for example, the fuel consumption of the afterburner is more than three times as high as the one of the primary burner. Any SFC improvements made by the technology level upgrades for the elements preceding the afterburner are thus nullified by the shear amount of fuel consumed during wet thrust.

What remains unclear are the circumstances which cause the base model, and to a small degree the VCE model, to underperform in terms of SFC at maximum thrust when upgrading to TL4 specifications. The results files also show that, despite the improvements to all components in terms of design performance data, the models have considerably worse resulting performance in terms of fan, compressor and turbine pressure ratios, lower air intake and lower net thrust output during wet thrust – maximum thrust in particular. At the design point however (maximum thrust), the switch from TL3 to TL4 improves the performance of the base model as expected. Why the performance is so markedly worsened in off-design mode at otherwise identical conditions is not readily apparent, but could possibly stem from the difference in how the models are controlled during design and off-design mode. In any case, the results for the TL-comparison in the particular case of wet thrust performance should be subject to scrutiny.

3.4 Envelope Sweep Data

In this section, the results for the SFC of both engine designs are presented in isoline/level plots with every point showing the SFC at a given Mach number and altitude. PLA is kept constant at 90. The SFC is in both cases presented as a percentage value of that of the base model. The first figure below, Figure 16, shows the SFC isolines for design 1. Take note that the colour schemes in the figures differ slightly from one another, i.e., the same colour in the two figures do not necessarily

represent the same percentage value.

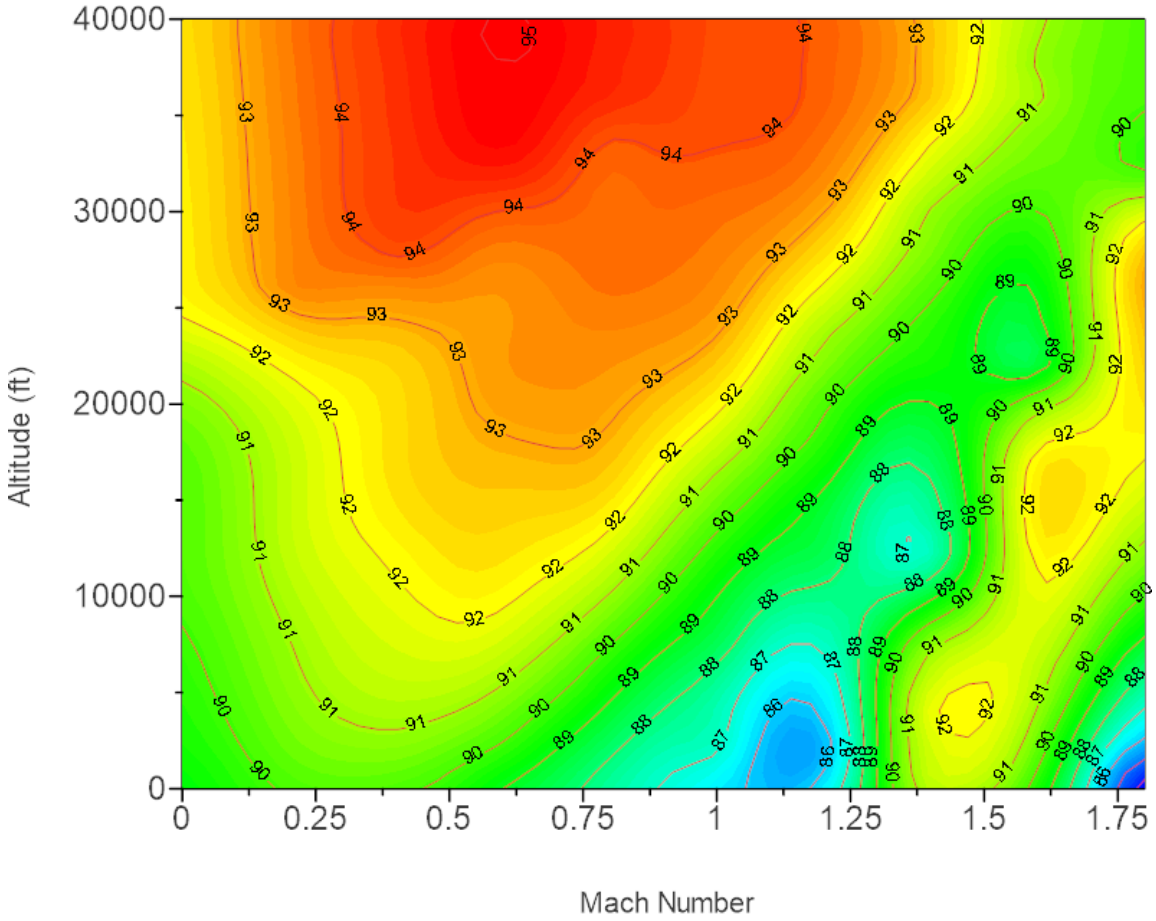

Figure 16: Level plot of design 1 SFC at PLA = 90 as a percentage share of the base model's for Mach numbers and altitudes ranging from 0 to 1.8 and 0 to 40 000 ft. respectively.

Apart from the points at the altitudes of 15 000 and 30 000 feet discussed in the previous section, the performance in terms of SFC can now be readily seen at higher and lower altitudes as well as higher and lower Mach numbers. Note however that the results for either very low velocities or very low altitudes are most likely not dependable, as operating points such as Mach 0 at a few hundred feet are not realistic. Also, since the PLA is being kept constant at 90, the points above Mach 1 should be viewed skeptically as flying at high supersonic speeds at part power is not very realistic. Since it is outside the scope of this thesis do determine where exactly the operational limits of the modelled engines lie, it was however decided to show the results in their entirety. The perhaps most important area of interest here is the portion of the plot that lies between the altitudes of 30 000 and 40 000 ft. and Mach numbers between 0.7 and 1, henceforth referred to as the cruise area, since these are the typical cruise points for the aircraft. For the cruise area, within which the aircraft will likely spend most of its flight time, the SFC lies rather steadily at 94 - 95 % of the base model's - a not insignificant improvement. Where this VCE design appears to perform particularly well however, is at low altitudes and while flying at high speeds at high altitude. Again however, keep in mind the lacking real life feasibility for some of these operating points. With consideration to the PLA and the infeasibility of certain combinations of Mach numbers and altitudes, the best performance improvement in terms of SFC is estimated to be found between the altitudes 10 000 and 15 000 ft. and around a velocity of Mach 0.9. This is congruent with the earlier results from the PLA sweeps.

The SFC isolines for design 2 are shown in Figure 17 below.

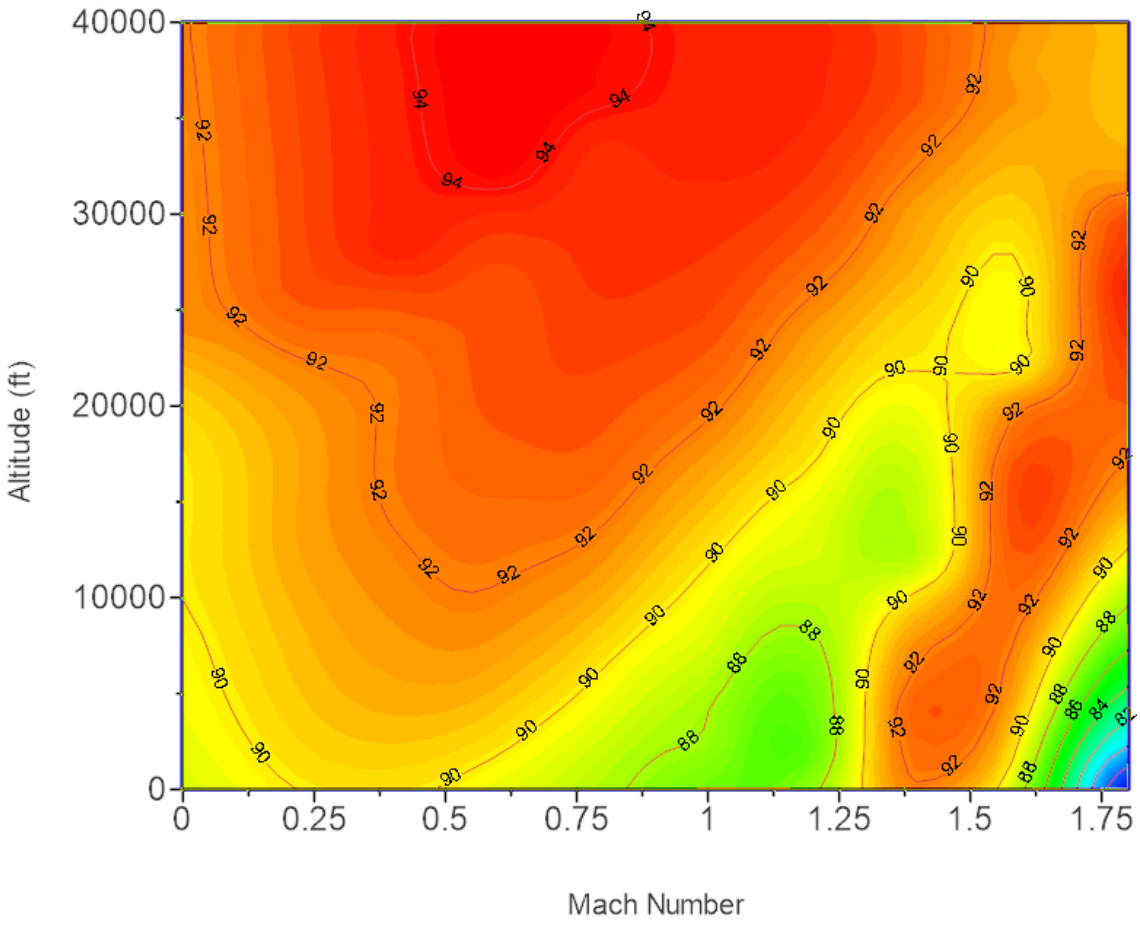

Figure 17: Level plot of design 2 SFC at PLA = 90 as a percentage share of the base model's for Mach numbers and altitudes ranging from 0 to 1.8 and 0 to 40 000 ft. respectively.

In this plot, it can be surmised that the performance in terms of SFC is very similar to that of design 1 in the cruise area. Other than that, the plot shows that design 2 has a slight edge over design 1 for most points at subsonic speed and altitude above 10 000 ft., with the SFC being a couple of percentage points lower than that of design 2 compared to the base model's. At supersonic speeds however, it is clear that design 1 performs better at most points. Again, taking the limitations to feasible operating points into account, it can be estimated that the largest improvement to SFC can be found between Mach 0.9 and 1 at an altitude of 10 000 ft. and lower.

3.5 Mission Analysis

This section handles the results for the Mission Sweep conducted for both VCE designs. The results of the sweep can be seen in Figure 18 below. The results for the fuel consumptions of the different models are shown as a percentage of the total fuel consumption accumulated by the base model. The plot of the base model fuel consumption is also included to get an understanding of during which different mission segments the fuel savings take place, although it may seem odd since at every point it represents a percentage of its own final fuel consumption.

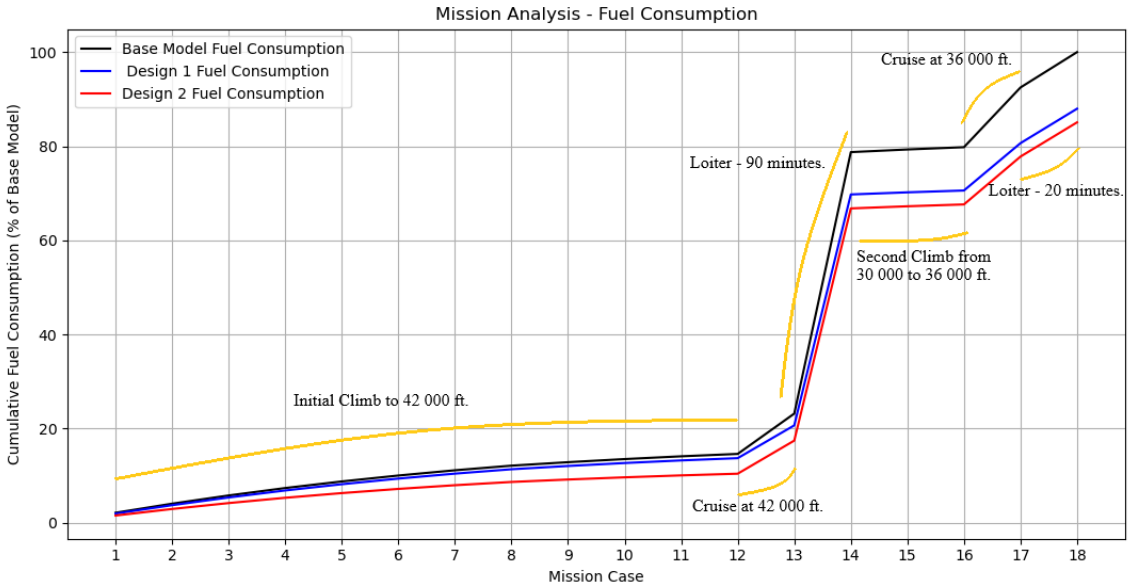

Figure 18: Accumulated total fuel consumption for the base model and the VCEs during the mission sweep. Shown as percentage of total fuel consumption for the base model.

From these results it is readily apparent that during a mission of this character, both VCE designs significantly outperform the base model in terms of fuel consumed. For design 1, the total fuel consumption amounts to ca. 89 % of the base model's, while the corresponding figure for design 2 is ca 86 %. Looking closer at the individual mission segments, it can be seen that most of the fuel savings are made during the initial climb for design 2, as well as the first 90 minute loiter for both VCE designs. Comparing to the results earlier shown in figures 9 and 12, this makes sense. During the second climb from 30 000 to 36 000 ft., the conditions for the engines are close to the ones seen in Figure 9 at Mach 0.7 and PLA 90, where both VCEs consume more than 10 % less fuel than the base model. At maximum wet thrust which is employed during the climb, design 2 is shown to significantly outperform the base model at all points so far tested while design 1 has similar SFC performance. During the loitering segment however, during which the aircraft is travelling at 30 000 ft. with a PLA of 70 and Mach 0.65, both designs are a marked improvement on the base model in terms of SFC.

4 Future Work

First and foremost, further time and energy would probably be well spent on resuming the work on modelling and controlling a VABI element. As earlier mentioned in the methodology chapter, a possible approach could be to this time try to specify a minimum air intake/front fan flow and have the VABI elements balance the total pressures in the mixing planes. This should make the VCE models work more akin to the three spool, separated flow VCE described earlier in the theoretical framework in terms of front fan flow maintained [3].

The second thing of interest would be to slightly change the VCE engine architecture with regard to the placement of the second mixer element. As stated in the methodology, the choice to mix the outer bypass flow with the core stream after the afterburner may have some negative impact on the engine performance in terms of both SFC and F_n while operating at wet thrust. One could also imagine work with further inspecting the actual effect that the present model configuration has on the infrared visibility of the exhaust plume, and thus determine the concrete pros and cons of this design choice. The engine architecture could also be modified to include two nozzles, similarly to Simmons' work described in the introduction section on VCEs. With this, obtaining convergence in the simulations would be made easier, and the engine could be made to operate more efficiently on lower power settings with higher obtainable bypass ratios. This should also be coupled with some sort of evaluation of the increased complexity that would come with the engine.

The different simulation sweeps that were included in this thesis would be more useful if it were known where the operating limits for the engines lie. Some examples of this would be the maximum flight velocities and altitudes attainable at different PLAs. Therefore, future work would do well to entail calculations for these limits. Furthermore, while the mission analysis that was conducted for this thesis gives a good indication on the potential benefits of a VCE within the analysed operating scope, the simplifications made and limitations imposed leaves some question marks. Diving further into the details by including segments such as the engine warmup and aircraft descents, not to mention re-expanding the scope of the mission to include supersonic flight segments, would give a more comprehensive and accurate analysis of the VCE designs.

Finally, work in the future on this subject could entail investigating the installation effects of the engine, which was omitted from the scope of this thesis.

5 Conclusion

The results show that both the VCE designs have clear advantages in terms of SFC compared to the base model, with the results obtained from the mission analysis performed showing possible fuel savings of ca. 11 and 14 % compared to the base model for VCE designs 1 and 2 respectively. The fuel savings were particularly impressive at low to medium altitudes and at cruise speeds. Compared to the base model, the SFC was also markedly improved for the second VCE design during wet thrust. The gains in SFC performance can be attributed to the increased bypass ratios possible during part power settings due to the VCE architecture. For both VCE designs, the performance gains made in terms of SFC came however at the price of decreased net thrust output at some points - primarily when operating at wet thrust. Lastly, the simulations done with TL4 component specifications for the first VCE design and the base model showed a large improvement to SFC, being as much as 20 and 28 % lower at part power settings respectively. At max power, the technology level made little to negligible difference.

The process of developing a VCE model came with several challenges. Firstly, arriving at a final design in regard to model layout and component design input data was rather time consuming due to the many target values that needed to be achieved, and restrictions that needed to be upheld. Changing one design value to achieve a better result for one parameter will adversely affect one or several others, and adding a new/different component may necessitate a complete reconfiguring of the model altogether. Another difficulty lay with the outer bypass channel specifically, in that it needed to allow for a relatively large airflow at part power while also being designed for max power at SLS conditions - that is, the BPR being set to a low value in design mode. The low values of the design Mach numbers that were set to allow for this made making any other changes in the model a sensitive affair, since the Mach numbers now had a narrower margin of possible values when running the simulations, and thus making convergence more difficult. The most difficult part no doubt however lay in the unfortunately abandoned of designing a VABI element and control schedule for the bypass ratio. In order for it to work, the design choice needs to be rethought. Instead of having the control schedule specify the BPR with the VABI adjusting the airflow accordingly, the control schedule could possibly be used to specify the air intake with the VABI balancing the total pressure in the mixing planes.

References

[1] Nicholas Cumpsty and Andrew Heyes. *Jet propulsion*. Cambridge University Press, 2015, p. 202.

[2] *Specific Fuel Consumption — grc.nasa.gov*. https://www.grc.nasa.gov/www/k-12/airplane/sfc.html. [Accessed 29-May-2023].

[3] J Johnson. "Variable cycle engine developments". In: *Developments in High-Speed-Vehicle Propulsion Systems* 165 (1995).

[4] Jeff Dahl. *Jet Engine*. CC BY-SA 4.0 <https://creativecommons.org/licenses/by-sa/4.0>, via Wikimedia Commons. Dec. 2007. URL: https://commons.wikimedia.org/wiki/File:Jet_engine.svg.

[5] Jack D Mattingly, Keith M Boyer, and Hans von Ohain. *Elements of propulsion: gas turbines and rockets*. American Institute of Aeronautics and Astronautics Reston, VA, 2006, pp. 372–373.

[6] K. Aainsqatsi. *Turbofan operation lbp*. CC BY-SA 4.0 <https://creativecommons.org/licenses/by-sa/4.0>, via Wikimedia Commons. May 2008. URL: https://commons.wikimedia.org/wiki/File:Turbofan_operation_lbp.svg.

[7] Philip P Walsh and Paul Fletcher. *Gas turbine performance*. John Wiley & Sons, 2004.

[8] JE Johnson. "Variable cycle engine concepts". In: *Np, nd Web* (1988).

[9] Ronald Jay Simmons. "Design and control of a variable geometry turbofan with and independently modulated third stream". PhD thesis. The Ohio State University, 2009.

[10] Southwest Research Institute. *NPSS User's Guide - v3.2*. Southwest Research Institute.

[11] The Ohio Aerospace Isntitute. *NPSS Thermodynamic Property Package User Guide - Software Release: NPSS 2.4.1*. 2012.

[12] Scott M Jones. *An introduction to thermodynamic performance analysis of aircraft gas turbine engine cycles using the numerical propulsion system simulation code*. Tech. rep. 2007.

[13] Southwest Research Institute. *Introduction to Propulsion Simulation Using NPSS*. Southwest Research Institute. 2018.

[14] NPSS Consortium. *NPSS User Guide Reference Sheets - Software Release: NPSS 3.2*. National Aeronautics and Space Administration (NASA). Oct. 2020.

[15] Herbert IH Saravanamuttoo, Gordon Frederick Crichton Rogers, and Henry Cohen. *Gas turbine theory*. Pearson education, 2001, pp. 121–123.

[16] Nidhi Baranwal and Shripad P. Mahulikar. "Review of Infrared signature suppression systems using optical blocking method". In: *Defence Technology* 15.3 (2019), pp. 432–439. ISSN: 2214-9147. DOI: https://doi.org/10.1016/j.dt.2018.12.002. URL: https://www.sciencedirect.com/science/article/pii/S2214914718303180.

[17] •. *MIL-STD-3013A - GLOSSARY OF DEFINITIONS, GROUND RULES, AND MISSION PROFILES TO DEFINE AIR VEHICLE PERFORMANCE CAPABILITY*. Tech. rep. Department of Defense, Sept. 2009.

[18] Jack D Mattingly. *Aircraft engine design*. Aiaa, 2002.

DEPARTMENT OF MECHANICS AND MARITIME SCIENCES
CHALMERS UNIVERSITY OF TECHNOLOGY
Gothenburg, Sweden 2023
www.chalmers.se

CHALMERS
UNIVERSITY OF TECHNOLOGY